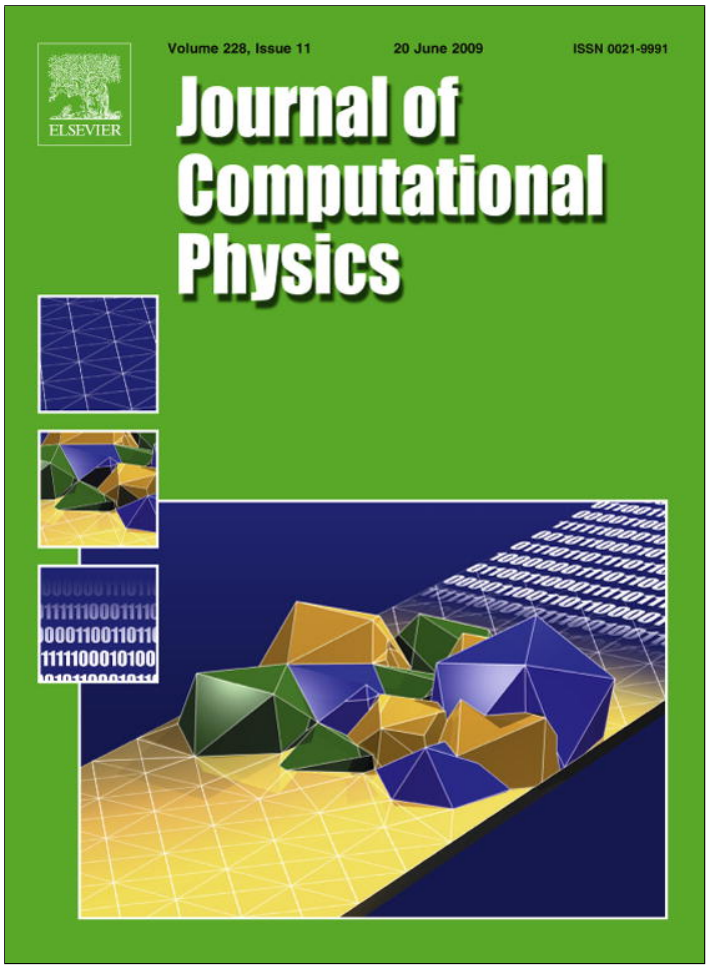

Journal of Computational Physics 228 (2009) 3973–3995

Contents lists available at ScienceDirect

Journal of Computational Physics

journal homepage: www.elsevier.com/locate/jcp

Gyro-water-bag approach in nonlinear gyrokinetic turbulence

Nicolas Besse [a,b,*], Pierre Bertrand [a]

[a] Institut Jean Lamour, UMR Nancy-Université CNRS 7198, Département Physique de la Matière et des Matériaux, Facult é des Sciences et Techniques, Université Henri Poincaré, Boulevard des Aiguillettes, B.P. 70239, 54506 Vandoeuvre-lès-Nancy Cedex, France
[b] Institut de Mathématiques Elie Cartan, UMR Nancy-Université CNRS INRIA 7502, Projet CALVIINRIA Grand Est, Faculté des Sciences et Techniques, Université Henri Poincaré, Boulevard des Aiguillettes, B.P. 70239, 54506 Vandoeuvre-lès-Nancy Cedex, France

ARTICLE INFO

Article history:
Received 26 October 2007
Received in revised form 16 February 2009
Accepted 17 February 2009
Available online 4 March 2009

AMS classification:
65M15
65P40
83C05

Keywords:
Water-bag model
Gyrokinetic equations
Quasilinear theory
Plasma turbulence
Discontinuous Galerkin methods
Semi-Lagrangian methods

ABSTRACT

Turbulent transport is a key issue for controlled thermonuclear fusion based on magnetic confinement. The thermal confinement of a magnetized fusion plasma is essentially determined by the turbulent heat conduction across the equilibrium magnetic field. It has long been acknowledged, that the prediction of turbulent transport requires to solve Vlasov-type gyrokinetic equations. Although the kinetic description is more accurate than fluid models (MHD, gyro-fluid), because among other things it takes into account nonlinear resonant wave–particle interaction, kinetic modeling has the drawback of a huge computer resource request. An unifying approach consists in considering water-bag-like weak solutions of kinetic collisionless equations, which allow to reduce the full kinetic Vlasov equation into a set of hydrodynamic equations, while keeping its kinetic behaviour. As a result this exact reduction induces a multi-fluid numerical resolution cost. Therefore finding water-bag-like weak solutions of the gyrokinetic equations leads to the birth of the gyro-water-bag model. This model is suitable for studying linear and nonlinear low-frequency micro-instabilities and the associated anomalous transport in magnetically-confined plasmas. The present paper addresses the derivation of the nonlinear gyro-water-bag model, its quasilinear approximation and their numerical approximations by Runge–Kutta semi-Lagrangian methods and Runge–Kutta discontinuous Galerkin schemes respectively.

1. Introduction

It is generally recognized that the anomalous transport observed in nonuniform magnetized plasmas is related to the existence of turbulent low-frequency electromagnetic fluctuations, i.e. with frequency much lower than the ion gyrofrequency. The presence of density, temperature and velocity gradients in the transverse direction of the magnetic confinement field, generates micro-instabilities which give rise to this turbulent transport. Low-frequency ion-temperature-gradient-driven (ITG) instability is one of the most serious candidates to account for the anomalous transport [43], as well as the so-called trapped electron modes (TEM) [38]. As the main energy loss in a controlled fusion devices is of conductive nature, the energy confinement time has the same order as the diffusion time a^2/χ_T where χ_T is the thermal diffusivity and "a" the transverse plasma size. Therefore it is crucial to determine this transport coefficient by computing the turbulent

* Corresponding author. Address: Institut Jean Lamour, UMR Nancy-Université CNRS 7198, Département Physique de la Matière et des Matériaux, Facult é des Sciences et Techniques, Université Henri Poincaré, Boulevard des Aiguillettes, B.P. 70239, 54506 Vandoeuvre-lès-Nancy Cedex, France. Tel.: +33 3 836 84902; fax: +33 3 836 84933.
E-mail addresses: besse@iecn.u-nancy.fr, Nicolas.Besse@lpmi.uhp-nancy.fr (N. Besse), Pierre.Bertrand@lpmi.uhp-nancy.fr (P. Bertrand).

0021-9991/$ - see front matter © 2009 Elsevier Inc. All rights reserved.
doi:10.1016/j.jcp.2009.02.025

nonlinear diffusivities in fusion plasmas. During recent years, ion turbulence in tokamaks has been intensively studied both with fluid (see for instance [17,23,34]) and gyrokinetic simulations using PIC codes [39,42,33] or Vlasov codes [14,25,16,11].

As far as the turbulent diffusion is concerned, it is commonly observed [18] that there exists a factor two between kinetic and fluid simulations ($\chi_{\text{fluid}} > 2\chi_{\text{kinetic}}$). Therefore the kinetic or fluid description may significantly impact the instability threshold as well as the predicted turbulent transport. The reasons of this observation is not really well understood: nonlinear Landau effects or nonlinear resonant wave–particle interaction, damping of poloidal velocity fluctuations, etc.

Consequently, it is important that gyrokinetic simulations measure the discrepancy between the local distribution function and a Maxwellian one, which is the main assumption of fluid closures.

In a recent paper [40] a comparison between fluid and kinetic approach has been addressed by studying a 3D kinetic interchange. A simple drift kinetic model is described by a distribution depending only on two spatial dimensions and parametrized by the energy. In that case it appears that the distribution function is far from a Maxwellian and cannot be described by a small number of moments. Wave–particle resonant processes certainly play an important role and most of the closures that have been developed will be inefficient.

On the other hand, although more accurate, the kinetic description of turbulent transport is much more demanding in computer resources than fluid simulations. This motivated us to revisit an alternative approach based on the water-bag-like weak solution of kinetic equations.

The water-bag model was introduced initially by DePackh [13], Hohl and co-workers [20,2,3], next extended to a double water-bag by Berk and Roberts [1] and finally generalized to the multiple water-bag by Finzi [21,37,4–6]. The water-bag model was shown to bring the bridge between fluid and kinetic description of a collisionless plasma, allowing to keep the kinetic aspect of the problem with the same complexity as a multi-fluid model. The aim of this paper is to use the water-bag description for gyrokinetic modeling.

After a brief introduction of the well known gyrokinetic equations hierarchy, we present the gyro-water-bag (GWB) model. We next derive a self-consistent quasilinear model, suitable for numerical simulation, in order to describe weak turbulence of magnetized plasmas in a cylinder. Therefore we propose numerical approximation schemes, one based on discontinuous Galerkin methods for solving the quasilinear equations, another based on semi-Lagrangian methods for solving the fully nonlinear equations. We then present some numerical results obtained in the context of plasma turbulence driven by ITG instabilities. Finally we make a comparison with results given by nonlinear and quasilinear simulations.

2. The gyro-water-bag model

2.1. The gyrokinetic equation

Predicting turbulent transport in collisionless fusion plasmas requires to solve the gyrokinetic equations for all species coupled to Darwin or Poisswell equations (low-frequency approximations of Maxwell equations in the asymptotic limit of infinite speed of light [7]). This gyrokinetic approach has been widely used in recent years to study low-frequency microinstabilities in a magnetically-confined plasma which are known for exhibiting a wide range of spatial and temporal scales. Gyrokinetic ordering employs the fact that the characteristic frequencies of the waves and gyroradii are small compared with the gyrofrequencies and unperturbed scale lengths, respectively, and that the perturbed parallel scale length is of the same order as the unperturbated scale length. Such an ordering enables one to be rid of the explicit dependence on the phase angle of the Vlasov equation through gyrophase-averaging while retaining the gyroradius effects to the arbitrary values of the gyroradius over the perturbated perpendicular scale length. The conventional approach [22] to derive the gyrokinetic Vlasov equation is based on a maximal multiple-scale-ordering expansion involving a single ordering parameter, which consists in computing an iterative solution of the gyroangle-averaged Vlasov equation perturbatively expanded in powers of a dimensionless parameter ρ/L, where ρ is the Larmor radius and L, the characteristic background magnetic field or plasma density and temperature nonuniformity length scale. A modern foundation of nonlinear gyrokinetic theory [19,26,9] is based on a two-step Lie-transform approach. The first step consists in the derivation of the guiding-center Hamilton equations, from the Hamiltonian particle dynamics, through the elimination of the gyroangle associated with the gyromotion time-scale of charged particles. If one takes into account finite gyroradius effects, one needs to reintroduce the gyroangle dependence into the perturbated guiding-center Hamiltonian dynamics which results that the magnetic moment μ is only conserved at first order in the dimensionless ordering parameter featuring electrostatic perturbations. Therefore one needs to perform a second-order perturbation analysis to derive the nonlinear gyrocenter dynamics. As a result, the second step consists in deriving a new set of gyrocenter Hamiltonian equations from the perturbated guiding-center equations, through a time-dependent gyrocenter phase-space transformation and gyroangle elimination. Finally, a reduced variational principle [10,9] enables one to derive self-consistent expressions for the nonlinear gyrokinetic Vlasov Maxwell equations. Within gyrokinetic Hamiltonian formalism, the Vlasov equation expresses the fact that the ions gyrocenter distribution function $f = f(t, \mathbf{r}, v_\parallel, \mu)$ is constant along gyrocenter characteristic curves in gyrocenter phase-space $(t, \mathbf{r}, v_\parallel, \mu)$:

$$D_t f = \partial_t f + \dot{X}_\perp \cdot \nabla_\perp f + \dot{X}_\parallel \cdot \nabla_\parallel f + \dot{v}_\parallel \partial_{v_\parallel} f = 0 \tag{1}$$

with

$$\dot{X}_\parallel = v_\parallel \mathbf{b}, \quad \dot{X}_\perp = v_{\mathbf{E}} + v_{\nabla B} + v_c,$$
$$\mathbf{v}_{\mathbf{E}} = \frac{1}{B^*_\parallel}\mathbf{b}\times\nabla\mathcal{J}_\mu\phi,$$
$$\mathbf{v}_{\nabla B} = \frac{\mu}{q_i B^*_\parallel}\mathbf{b}\times\nabla B,$$
$$\mathbf{v}_c = \frac{m_i v_\parallel^2}{q_i B^*_\parallel}\left(\frac{\mathbf{b}\times\nabla B}{B} + \frac{(\nabla\times\mathbf{B})_\perp}{B}\right) = \frac{m_i v_\parallel^2}{q_i B^*_\parallel}\mathbf{b}\times\frac{\mathbf{N}}{R_c},$$
$$\dot{v}_\parallel = -\frac{1}{m_i}\left(\mathbf{b} + \frac{m_i v_\parallel}{q_i B^*_\parallel}\mathbf{b}\times\frac{\mathbf{N}}{R_c}\right)\cdot(\mu\nabla B + q_i\nabla\mathcal{J}_\mu\phi),$$
$$\mathbf{B}^* = \mathbf{B} + \frac{m_i v_\parallel}{q_i}\nabla\times\mathbf{b}, \quad B^*_\parallel = \mathbf{B}^*\cdot\mathbf{b},$$

where $\mathbf{b} = \mathbf{B}/B$ denotes the unit vector along magnetic field line, $\mathcal{J}_\mu$ denotes the gyroaverage operator, $\mathbf{N}/R_c$ is the field line curvature, $q_i = Z_i e, e > 0$ being the electron Coulomb charge, and $\mu = m_i v_\perp^2/(2B)$ is the first adiabatic invariant of the ion gyrocenter. The structure of the distribution function f, solution of (1), is of the form

$$f(t,\mathbf{r},v_\parallel,\mu) = \sum_\ell f_\ell(t,\mathbf{r},v_\parallel)\delta(\mu-\mu_\ell). \tag{2}$$

Let us notice that it is an interesting problem to know what is the asymptotic statistical distribution function in μ in (2) if we consider an infinite number of magnetic moments, because it allows to save CPU time and memory space in numerical codes. In [27,31,32], the authors take the distribution $m_i\exp(-\mu B/T_{i0})/T_{i0}$. If we now assume that the background distribution is Maxwellian in μ with temperature T_{i0} and linearly varying density n_{i0}, then after linearization around the background distribution ($n_i = n_{i0} + \delta n_i, \delta n_i/n_{i0} \sim \varepsilon_\delta \ll 1$) the Fourier transformed Poisson equation becomes

$$\left\{|\mathbf{k}|^2\lambda_{D_i}^2 + 1 - \Gamma_0(b) - [\Gamma_1(b)-\Gamma_0(b)]i\mathbf{k}_\perp\cdot(\rho_i^2\nabla_\perp\ln n_{i0})\right\}Z_i q_i\frac{n_{i0}}{k_B T_{i0}}\phi_{\mathbf{k}} = Z_i\int J_0\left(k_\perp\sqrt{\frac{2\mu}{\Omega_i q_i}}\right)f_{\mathbf{k}}2\pi\frac{\Omega_i}{q_i}d\mu dv_\parallel - n_{e\mathbf{k}}, \tag{3}$$

where $\rho_i^2 = v_{thi}^2/\Omega_i^2 = k_B T_i/(m_i\Omega_i^2)$ is the ion Larmor radius, $b = k_\perp^2\rho_i^2, \lambda_{D_i}^2 = k_B T_i/(4\pi\varepsilon_0 Z_i^2 e^2 n_{i0})$ is the ion Debye length, $\Gamma_n(b) = I_n(b)\exp(-b)$, I_n is a modified Bessel function of order n, and where J_0 is a Bessel function of zero order. Eq. (3) describes linear drift waves for $k_\perp\rho_i = \mathcal{O}(1)$ and nonlinear drift waves for small $k_\perp\rho_i$. Firstly we are interested in the effects of the transversal drift velocity $\mathbf{E}\times\mathbf{B}$ coupled to the parallel dynamics while the curvature effects are considered as a next stage of the study. As a result, in the sequel we deal with a reduced gyrokinetic model in cylindrical geometry by making the following approximations:

- In addition of cylindrical geometry, we suppose that the magnetic field $\mathbf{B}$ is uniform and constant along the axis of the column (z-coordinate, $\mathbf{B} = B\mathbf{b} = B\mathbf{e}_z$). It follows the perpendicular drift velocity does not admit any magnetic curvature or gradient effect and especially $\mathbf{B}^* = \mathbf{B}$.
- We suppose that we have a finite discrete sequence of adiabatic invariant $\Xi = \{\mu\}$ linked to a finite discrete sequence of ion Larmor radius $\Lambda = \{\rho\}$ by $\mu = \rho^2\Omega_i q_i/2$. Since the gyroaverage linear differential operator $\mathcal{J}_\mu$ becomes the Bessel function $J_0(k_\perp\sqrt{2\mu}/\sqrt{\Omega_i q_i})$ in the Fourier space, if we suppose $k_\perp\rho$ small ($k_\perp\rho \lesssim 1$) then we can use the approximation

$$J_0(k_\perp\rho) = 1 - \frac{k_\perp^2\rho^2}{4} + \mathcal{O}(k_\perp^4\rho^4) = \frac{1}{1+\frac{k_\perp^2\rho^2}{4}} + \mathcal{O}(k_\perp^4\rho^4),$$

which means in term of differential operator that we make the approximation

$$\mathcal{J}_\mu \sim \left(1 - \frac{\rho^2}{4}\Delta\right)^{-1}. \tag{4}$$

- We linearize the left hand side of Eq. (3) by considering $k_\perp\rho_i$ small and neglecting all terms smaller than $\mathcal{O}(k_\perp^2\rho_i^2)$. Moreover we assume that the ion Debye length λ_{D_i} is small compared to the ion Larmor radius ρ_i and we suppose that Ω_i is a constant Ω_0.
- The electron inertia is ignored, i.e. we choose and adiabatical response to the low-frequency fluctuations for the electrons. In other words the electron density follows the Boltzmann distribution:

$$n_e = n_{e0}\exp\left(\frac{e}{k_B T_e}(\phi - \lambda\langle\phi\rangle_{\mathcal{M}})\right),$$

where $\langle\phi\rangle_{\mathcal{M}}$ denotes the average of the electrical potential ϕ over a magnetic surface. Moreover we assume that the electrical potential is small compared to the electron kinetic energy $e\phi/(k_B T_e) \sim \varepsilon_\delta \ll 1$.

Under these assumptions the evolution of the sequence of ion guiding-center distribution functions $f_\mu = f_\mu(t, \mathbf{r}_\perp, z, v_\parallel)$ obeys the gyrokinetic Vlasov equations (see [25] for more details)

$$\partial_t f_\mu + \mathcal{J}_\mu \mathbf{v}_\mathbf{E} \cdot \nabla_\perp f_\mu + v_\parallel \partial_z f_\mu + \frac{q_i}{m_i} \mathcal{J}_\mu E_\parallel \partial_{v_\parallel} f_\mu = 0, \quad \forall \mu \in \Xi, \tag{5}$$

for the ions (q_i, M_i), coupled to an adiabatic electron response via the quasineutrality assumption

$$-\nabla_\perp \cdot \left(\frac{n_{i0}}{B\Omega_0} \nabla_\perp \phi \right) + \frac{e\tau n_{i0}}{k_B T_{i0}} (\phi - \lambda \langle \phi \rangle_{\mathcal{M}}) = 2\pi \sum_{\mu \in \Xi} \int_{\mathbb{R}} \frac{\Omega_i}{q_i} \mathcal{J}_\mu f_\mu(t, \mathbf{r}, v_\parallel) dv_\parallel - n_{i0}. \tag{6}$$

Here $q_i = Z_i e, Z_i n_{i0} = n_{e0}, T_e = T_{e0}, \tau = T_{i0}/T_{e0}, \lambda \in \{0, 1\}, \mathbf{E} = -\nabla\phi$ and $\mathbf{v}_\mathbf{E}$ is the $\mathbf{E} \times \mathbf{B}/B^2$ drift velocity. The most important and interesting feature is that f_μ depends, through a differential operator, only on the velocity component $v_\parallel$ parallel to $\mathbf{B}$.

2.2. The gyro-water-bag model (GWB)

Let us now turn back to the gyrokinetic equation (5). Since the distribution $f_\mu(t, \mathbf{r}_\perp, z, v_\parallel)$ takes into account only one velocity component $v_\parallel$, a water-bag solution can be considered [4]. For each adiabatic invariant $\mu \in \Xi$, let us consider $2\mathcal{N}$ ordered non closed contours in the $(\mathbf{r}, v_\parallel)$-phase-space labelled $v^+_{\mu j}$ and $v^-_{\mu j}$ (where $j = 1, \ldots, \mathcal{N}$) such that $\cdots < v^-_{\mu j+1} < v^-_{\mu j} < \cdots < 0 < \cdots < v^+_{\mu j} < v^+_{\mu j+1} < \cdots$ and some strictly positive real numbers $\{\mathcal{A}_{\mu j}\}_{j \in [1,\mathcal{N}],\ \mu \in \Xi}$ that we call bag heights. We then define the distribution function $f_\mu(t, \mathbf{r}_\perp, z, v_\parallel)$ as

$$f_\mu(t, \mathbf{r}_\perp, z, v_\parallel) = \sum_{j=1}^{\mathcal{N}} \mathcal{A}_{\mu j} \left[\mathcal{H}(v_\parallel - v^-_{\mu j}(t, \mathbf{r}_\perp, z)) - \mathcal{H}\Big(v_\parallel - v^+_{\mu j}(t, \mathbf{r}_\perp, z) \Big) \right], \tag{7}$$

where $\mathcal{H}$ is the Heaviside unit step function. The function (7) is an exact solution of the gyrokinetic Vlasov equation (5) in the sense of distribution theory, if and only if the set of following equations are satisfied:

$$\partial_t v^\pm_{\mu j} + \mathcal{J}_\mu \mathbf{v}_\mathbf{E} . \nabla_\perp v^\pm_{\mu j} + v^\pm_{\mu j} \partial_z v^\pm_{\mu j} = \frac{q_i}{m_i} \mathcal{J}_\mu E_\parallel, \quad j \in [1, \mathcal{N}], \quad \forall \mu \in \Xi. \tag{8}$$

The quasineutrality coupling (6) can be rewritten as

$$-\nabla_\perp \cdot \left(\frac{n_{i0}}{B\Omega_0} \nabla_\perp \phi \right) + \frac{e\tau n_{i0}}{k_B T_{i0}} (\phi - \lambda \langle \phi \rangle_{\mathcal{M}}) = 2\pi \sum_{\mu \in \Xi} \sum_{j=1}^{\mathcal{N}} \frac{\Omega_i}{q_i} \mathcal{A}_{\mu j} \mathcal{J}_\mu (v^+_{\mu j} - v^-_{\mu j}) - n_{i0}. \tag{9}$$

Let us introduce for each bag j the density $n_{\mu j} = (v^+_{\mu j} - v^-_{\mu j}) \mathcal{A}_{\mu j}$ and the average velocity $u_{\mu j} = (v^+_{\mu j} + v^-_{\mu j})/2$. After little algebra, Eq. (8) lead to continuity and Euler equations namely

$$\partial_t n_{\mu j} + \nabla_\perp \cdot (n_{\mu j} \mathcal{J}_\mu \mathbf{v}_\mathbf{E}) + \partial_z (n_{\mu j} u_{\mu j}) = 0, \quad \partial_t (n_{\mu j} u_{\mu j}) + \nabla_\perp \cdot (n_{\mu j} u_{\mu j} \mathcal{J}_\mu \mathbf{v}_\mathbf{E}) + \partial_z \left(n_{\mu j} u^2_{\mu j} + \frac{p_{\mu j}}{m_i} \right) = \frac{q_i}{m_i} n_{\mu j} \mathcal{J}_\mu E_\parallel,$$

where the partial pressure takes the form $p_{\mu j} = m_i n^3_{\mu j} / (12 \mathcal{A}^2_{\mu j})$.

The connection between kinetic and fluid description clearly appears in the previous multi-fluid equations. The case of one bag recovers a fluid description (with an exact adiabatic closure with $\gamma = 3$) and the limit of an infinite number of bags provides a continuous distribution function.

2.3. Normalization and conservation laws

The numerical schemes developed in a forthcoming section are based on normalized equations. In our case, the temperature T_{i0} and T_{e0} are normalized to a characteristic temperature $\overline{T}_0$, which is defined such that $T_{i0}(r_0)/\overline{T}_0 = 1$. The longitudinal direction is normalized to $k_\parallel$, the characteristic fluctuation parallel wavenumber and the transversal direction to $k_\perp$, the characteristic fluctuation perpendicular wavenumber. The velocity is normalized to the ion thermal velocity $v_{thi} = \sqrt{T_{i0}/m_i}$ and the time to characteristic fluctuation frequency $\omega^{-1} = (k_\parallel v_{thi})^{-1}$. Finally the electrical potential ϕ is normalized to the characteristic fluctuation potential $\overline{\phi}$. Moreover we define the dimensionless ordering parameters

$$\varepsilon_k = \frac{k_\parallel}{k_\perp}, \quad \varepsilon_\omega = \frac{\omega}{\Omega_0}, \quad \varepsilon_\delta = \frac{e\overline{\phi}}{k_B \overline{T}_0}, \quad \varepsilon_{\nabla_{eq}} = \frac{\rho_i}{L_{\nabla_{eq}}}, \quad \varepsilon_\perp = \rho_i k_\perp, \tag{10}$$

where ρ_i is ion Larmor radius and $L_{\nabla_{eq}}$ is the characteristic background plasma density and temperature nonuniformity length scale. The gyrokinetic ordering is achieved for $\varepsilon_k \sim \varepsilon_\omega \sim \varepsilon_\delta \sim \varepsilon_{\nabla,eq} \sim \varepsilon \sim 10^{-3}$ and $\varepsilon_\perp \sim 1$. For longer wavelengths such that $\varepsilon_\perp \ll 1$ we obtain the drift kinetic ordering. Using the dimensionless ordering parameters (10), Eqs. (8) and (9) become

$$\partial_t v^\pm_{\mu j} + \varepsilon_\delta \varepsilon_\omega \varepsilon_k^{-2} Z_i (\mathbf{e}_z \times \nabla \mathcal{J}_\mu \phi) \cdot \nabla_\perp v^\pm_{\mu j} + v^\pm_{\mu j} \partial_z v^\pm_{\mu j} = Z_i \varepsilon_\delta \mathcal{J}_\mu E_\parallel \tag{11}$$

and

$$-\varepsilon_\delta\varepsilon_\omega^2\varepsilon_k^{-2}Z_i\nabla_\perp\cdot(n_{i0}\nabla_\perp\phi)+\frac{\varepsilon_\delta\tau n_{i0}}{T_{i0}}(\phi-\lambda\langle\phi\rangle_{\mathcal{M}})=2\pi\sum_{\mu\in\Xi}\sum_{j=1}^{\mathcal{N}}\mathcal{A}_{\mu j}\mathcal{J}_\mu(v_{\mu j}^+-v_{\mu j}^-)-n_{i0}. \tag{12}$$

The system (11) and (12) preserves some physical quantities such as the total number of particle

$$\sum_{\mu j}\mathcal{A}_{\mu j}\int d\mathbf{r}(v_{\mu j}^+-v_{\mu j}^-)$$

and the total energy

$$\sum_{\mu j}\mathcal{A}_{\mu j}\int d\mathbf{r}\left(\mu(v_{\mu j}^+-v_{\mu j}^-)+\frac{v_{\mu j}^{+3}}{6}-\frac{v_{\mu j}^{-3}}{6}\right)+\int d\mathbf{r}\left(2\pi\sum_{\mu j}\mathcal{A}_{\mu j}\mathcal{J}_\mu(v_{\mu j}^+-v_{\mu j}^-)-n_{i0}\right)\phi, \tag{13}$$

where in the definition (13) the first term denotes the kinetic energy and the second one is the potential energy. Finally we define the heat flux at a radial position r and a time t as the quantity

$$Q(t,r)=\sum_{\mu j}\mathcal{A}_{\mu j}\int\frac{d\theta}{2\pi}\frac{dz}{L_z}\left(\mu(v_{\mu j}^+-v_{\mu j}^-)+\frac{v_{\mu j}^{+3}}{6}-\frac{v_{\mu j}^{-3}}{6}\right)(\mathbf{e}_z\times\nabla\mathcal{J}_\mu\phi)\cdot\mathbf{e}_r.$$

3. Derivation of a self-consistent quasilinear gyro-water-bag model

In this section we shall derive a self-consistent quasilinear system suitable for numerical approximation. This model will be useful to make comparison with the nonlinear model, in the linear and quasilinear regime. Every unknown is expanded as

$$f(t,r,\theta,z)=\frac{1}{2}\left\{f_0(t,r,z)+\sum_{m>0}f_m(t,r,z)e^{i\theta m}\right\}+\text{c.c.}, \tag{14}$$

where f_0 is a real number and f_m is a complex number. Introducing the expansion (14) into Eq. (8) and assuming the limit $k_\perp\rho\to 0(\mathcal{J}_\mu\to 1)$, after some algebra we obtain

$$\partial_t v_{j0}^\pm+\partial_z\left(\frac{v_{j0}^{\pm\,2}}{2}+\phi_0\right)+\frac{1}{2rB}\sum_{m>0}m\partial_r(V_{jm}^\pm\times\Phi_m)+\frac{1}{4}\sum_{m>0}\partial_z(|V_{jm}^\pm|^2)=0, \tag{15}$$

$$\partial_t V_{jm}^\pm+\frac{1}{r}\partial_r(r\mathcal{H}_m)V_{jm}^\pm-\frac{1}{r}\partial_r(r\mathcal{K}_{jm}^\pm)\Phi_m+\partial_z(v_{j0}^\pm V_{jm}^\pm+\Phi_m)+\mathcal{F}=0, \tag{16}$$

where

$$\mathcal{H}_m=\frac{m}{Br}\phi_0\mathcal{I},\quad \mathcal{K}_{jm}^\pm=\frac{m}{Br}v_{j0}^\pm\mathcal{I},\quad \mathcal{I}=\begin{pmatrix}0&-1\\1&0\end{pmatrix},\quad V_{jm}^\pm=\begin{pmatrix}\mathfrak{Re}\,v_{jm}^\pm\\ \mathfrak{Im}\,v_{jm}^\pm\end{pmatrix},\quad \Phi_m=\begin{pmatrix}\mathfrak{Re}\,\phi_m\\ \mathfrak{Im}\,\phi_m\end{pmatrix},\quad \mathcal{F}=\begin{pmatrix}\mathcal{F}_1\\ \mathcal{F}_2\end{pmatrix}$$

with

$$\begin{aligned}\mathcal{F}_1=&\frac{1}{2Br}\sum_\ell m\left(\partial_r\Phi_\ell\mathbin{\widehat{\times}}V_{jm-\ell}^\pm\right)+m\left(\partial_r\Phi_{m+\ell}\times V_{j\ell}^\pm\right)+m\left(V_{jm+\ell}^\pm\times\partial_r\Phi_\ell\right)+\ell\partial_r\left(V_{jm+\ell}^\pm\times\Phi_\ell\right)-(\ell+m)\partial_r\left(\Phi_{m+\ell}\times V_{j\ell}^\pm\right)\\&-\ell\partial_r\left(\Phi_\ell\mathbin{\widehat{\times}}V_{jm-\ell}^\pm\right)+\sum_\ell\frac{1}{4}\partial_z\left(V_{j\ell}^\pm\mathbin{\hat{\cdot}}V_{jm-\ell}^\pm\right)+\frac{1}{2}\partial_z\left(V_{j\ell}^\pm\cdot V_{jm+\ell}^\pm\right)\end{aligned} \tag{17}$$

and

$$\begin{aligned}\mathcal{F}_2=&\frac{1}{2Br}\sum_\ell m\left(\partial_r\Phi_\ell\mathbin{\hat{\cdot}}V_{jm-\ell}^\pm\right)+m\left(\partial_r\Phi_{m+\ell}\cdot V_{j\ell}^\pm\right)+m\left(V_{jm+\ell}^\pm\cdot\partial_r\Phi_\ell\right)+\ell\partial_r\left(V_{jm+\ell}^\pm\cdot\Phi_\ell\right)-(\ell+m)\partial_r\left(\Phi_{m+\ell}\cdot V_{j\ell}^\pm\right)\\&-\ell\partial_r\left(\Phi_\ell\mathbin{\hat{\cdot}}V_{jm-\ell}^\pm\right)+\sum_\ell\frac{1}{4}\partial_z\left(V_{j\ell}^\pm\mathbin{\widehat{\times}}V_{jm-\ell}^\pm\right)+\frac{1}{2}\partial_z\left(V_{j\ell}^\pm\times V_{jm+\ell}^\pm\right).\end{aligned} \tag{18}$$

In Eqs. (17) and (18) we have used the notations $U\mathbin{\hat{\cdot}}V=U_1V_1-U_2V_2$, $U\mathbin{\widehat{\times}}V=U_1V_2+U_2V_1$, where U and V are two-dimensional vectors. The quadratic nonlinear terms in $V_{jm}^\pm$, which lead to the coupling of modes and to the existence of a saturation regime will be neglected in (16) and kept in Eq. (15). In other words, the term $\mathcal{F}$ is dropped in Eq. (16). Using the dimensionless ordering parameters (10), Eqs. (15) and (16), in the dimensionless form become

$$\partial_t v_{j0}^\pm+\partial_z\left(\frac{v_{j0}^{\pm\,2}}{2}+Z_i\varepsilon_\delta\phi_0\right)+\sum_{m>0}\varepsilon_\delta\varepsilon_\omega\varepsilon_k^{-2}Z_i\frac{m}{2r}\partial_r\left(V_{jm}^\pm\times\Phi_m\right)+\sum_{m>0}\partial_z\left(\frac{|V_{jm}^\pm|^2}{4}\right)=0, \tag{19}$$

$$\partial_t V_{jm}^\pm+\varepsilon_\delta\varepsilon_\omega\varepsilon_k^{-2}Z_i\frac{1}{r}\left\{\partial_r(r\mathcal{H}_m)V_{jm}^\pm-\partial_r(r\mathcal{K}_{jm}^\pm)\Phi_m\right\}+\partial_z(v_{j0}^\pm V_{jm}^\pm+Z_i\varepsilon_\delta\Phi_m)=0. \tag{20}$$

Substituting the expansion (14) into Eq. (9) and using the ordering dimensionless parameters (10), we obtain the dimensionless equations

$$-\varepsilon_\delta\varepsilon_k^{-2}\varepsilon_\omega^2 Z_i\frac{1}{r}\partial_r(rn_{i0}\partial_r\phi_0)+\frac{\varepsilon_\delta\tau n_{i0}}{T_{i0}}(\phi_0-\lambda\langle\phi_0\rangle_{\mathcal{M}})=\sum_{j=1}^{\mathcal{N}}\mathcal{A}_j(v_{j0}^+-v_{j0}^-)-n_{i0} \tag{21}$$

and

$$-\varepsilon_\delta\varepsilon_k^{-2}\varepsilon_\omega^2 Z_i\frac{1}{r}\partial_r(rn_{i0}\partial_r\Phi_m)+\left(\varepsilon_\delta\varepsilon_\omega^2\varepsilon_k^{-2}Z_i\frac{m^2}{r^2}+\frac{\varepsilon_\delta\tau n_{i0}}{T_{i0}}\right)\Phi_m=\sum_{j=1}^{\mathcal{N}}\mathcal{A}_j(V_{jm}^+-V_{jm}^-). \tag{22}$$

Finally we are interested to solve the system formed by Eqs. (19)–(22).

4. Numerical approximation

This section is devoted to the numerical resolution of the fully nonlinear model (11) and (12), and the self-consistent quasilinear model (19)–(22). Although these two models are different they should give the same results (the same growth rate value of the ITG instability) in the linear regime. In order to cross-check the models and the numerical schemes, we decide to solve every system by a different numerical method. The quasilinear model (19)–(22) is solved by using a forward Runge–Kutta discontinuous Galerkin method while a backward Runge–Kutta semi-Lagrangian method is chosen to discretize the nonlinear system (19)–(22).

4.1. Numerical approximation of the nonlinear system

In this section we present the numerical method to solve the Eqs. (11) and (12), where, without loss of generality, only one adiabatic invariant $\mu=\mu_0$ is considered. For the sake of clarity we drop the index μ. The scheme is based on a backward Runge–Kutta semi-Lagrangian method. If we introduce the characteristic curves $\mathbf{r}_j^\pm(t)=(r_j^\pm(t),\theta_j^\pm(t),z_j^\pm(t))$ associated to the transport first-order differential operator

$$\partial_t+\varepsilon_\delta\varepsilon_\omega\varepsilon_k^{-2}Z_i(\mathbf{e}_z\times\nabla\mathcal{J}_\mu\phi)\cdot\boldsymbol{\nabla}_\perp+v_{\mu j}^\pm\partial_z,$$

then, for $j=1,\dots,\mathcal{N}$, Eq. (11) can be rewritten as

$$\frac{d}{dt}v_j^\pm(t,\mathbf{r}_j^\pm(t))=Z_i\varepsilon_\delta\mathcal{J}E_\parallel(t,\mathbf{r}_j^\pm(t)),\quad v_j^\pm(0)=v_j^{\pm0}, \tag{23}$$

where

$$\frac{d}{dt}\mathbf{r}_j^\pm(t)=F(t,\mathbf{r}_j^\pm(t),\mathcal{J}\phi(t),v_j^\pm(t)) \tag{24}$$

with

$$F(t,\mathbf{r},\mathcal{J}\phi,u)=\begin{pmatrix}-\frac{\eta}{r}\partial_\theta\mathcal{J}\phi(t,\mathbf{r})\\ \frac{\eta}{r}\partial_r\mathcal{J}\phi(t,\mathbf{r})\\ u(t,\mathbf{r})\end{pmatrix}\quad\text{and}\quad\eta=Z_i\varepsilon_\delta\varepsilon_\omega\varepsilon_k^{-2}.$$

Let be Ω the domain of computation and $\mathcal{M}_h$ a partition of Ω, of element K such that $K=K_{i_r+\frac12,i_\theta+\frac12,i_z+\frac12}=\left\{(r,\theta,z)||r-r_{i_r+\frac12}|\leqslant\right.$ $\Delta r/2,|\theta-\theta_{i_\theta+\frac12}|\leqslant\Delta\theta/2,|z-z_{i_z+\frac12}|\leqslant\Delta z/2\}$ where $\Delta r=L_r/N_r,\Delta\theta=2\pi/N_\theta$ and $\Delta z=L_z/N_z$, are the spatial discretization parameters. We now seek an approximate solution $(v_{hj}^\pm,\phi_h)\in(\mathcal{C}^2\cap\mathfrak{B}_{4,h}(\Omega))^{\otimes^3}$, for each value of the time variable and for $j=1,\dots,\mathcal{N}$, where

$$\mathfrak{B}_{4,h}(\Omega)=\mathcal{S}_{4,\Delta r}^c(\{s_i\}_{i=0\dots N_r},s_0',s_1')\otimes\mathcal{S}_{4,\Delta\theta}^p(\{s_i\}_{i=0\dots N_\theta})\otimes\mathcal{S}_{4,\Delta z}^p(\{s_i\}_{i=0\dots N_z})$$

with

$$\mathcal{S}_{4,\Delta x}^p(\{s_i\}_{i=0\dots N_x})=\left\{\begin{array}{l}s(x)\in\mathcal{C}^2([x_0,x_{N_x}]),\ s_{|[x_i,x_{i+1}]}\in\mathcal{P}_3,\ \forall i\in[0,N_x-1];\\ D^4s(x)=0,\ \forall x\in(x_i,x_{i+1}),\ \forall i\in[0,N_x-1];\\ s^{(k)}(x_0)=s^{(k)}(x_{N_x}),\ k=0,\dots,2,\ s(x_i)=s_i,\ \forall i\in[0,N_x].\end{array}\right\}$$

and

$$\mathcal{S}_{4,\Delta x}^c(\{s_i\}_{i=0\dots N_x},s_0',s_1')=\left\{\begin{array}{l}s(x)\in\mathcal{C}^2([x_0,x_{N_x}]),\ s_{|[x_i,x_{i+1}]}\in\mathcal{P}_3,\ \forall i\in[0,N_x-1];\\ s(x)=\arg\min\limits_{\substack{f\in\mathcal{C}^2\\ f\neq0}}\left(\int_{x_0}^{x_{N_x}}|D^2f|^2\right);\\ s'(x_0)=s_0',\ s'(x_{N_x})=s_1',\ s(x_i)=s_i,\ \forall i\in[1,N_x-1].\end{array}\right\}.$$

Therefore a three-dimensional cubic-spline s_f which interpolates f at the points $\{r_{i_r}, \theta_{i_\theta}, z_{i_z}\}_{i_r=0\ldots N_r, i_\theta=0\ldots N_\theta, i_z=0\ldots N_z}$ with boundary conditions can be expanded as follows:

$$s_f(r,\theta,z) = \sum_{i_r=-1}^{N_r+1}\sum_{i_\theta=-1}^{N_\theta+1}\sum_{i_z=-1}^{N_z+1} c_{i_r i_\theta i_z}(f) B^4(r/\Delta r - i_r) B^4(\theta/\Delta\theta - i_\theta) B^4(z/\Delta z - i_z),$$

where the coefficient set $\{c_{i_r i_\theta i_z}(f)\}_{i_r=-1\ldots N_r+1, i_\theta=-1\ldots N_\theta+1, i_z=-1\ldots N_z+1}$ solve a linear system determined by interpolation constraints and boundary conditions, and where $B^4 = B*B*B*B$ with $B(x) = 1$ if $x \in [-1/2, 1/2]$ and zero elsewhere. After space discretization the ordinary differential system (23) and (24) becomes

$$\begin{aligned} &\frac{d}{dt} v_{h,j}^{\pm}(t, \mathbf{r}_{h,j}^{\pm}(t)) = Z_i \varepsilon_\delta \mathcal{J}^h E_{h\|}(t, \mathbf{r}_{h,j}^{\pm}(t)), \quad v_{h,j}^{\pm}(0) = v_{h,j}^{\pm 0}, \\ &\frac{d}{dt}\mathbf{r}_{h,j}^{\pm}(t) = F_h(t, \mathbf{r}_{h,j}^{\pm}(t), \mathcal{J}^h\phi_h(t), v_{h,j}^{\pm}(t)), \end{aligned} \tag{25}$$

where $\mathbf{r}_{h,j}^{\pm}(t)$ is an approximation of the exact characteristic curve $\mathbf{r}_j^{\pm}(t)$, $\mathcal{J}^h$ is a numerical approximation (Eq. (34)) of the gyroaverage operator $\mathcal{J}$ (Eq. (4)), and F_h is an approximation of the vector field F. Let be $\Delta t = T/N_T$ the time discretization parameter, thus the ordinary differential equations (25) are approximated in time by the following second-order backward Runge–Kutta method. For all $n \in [0, N_T - 1], j \in [0, \mathcal{N}], \mathbf{k} = (r_{i_r}, \theta_{i\theta}, z_{i_z}) \in \Sigma = [0, N_r] \times [0, N_\theta] \times [0, N_z]$ we imposed that

Step 1:

$$\begin{aligned} &v_{h,j}^{\pm n+1/2}\left(\mathbf{r}_{h,j}^{\pm n+1/2}\right) = v_{h,j}^{\pm n}\left(\mathbf{r}_{h,j}^{\pm n}\right) + Z_i\varepsilon_\delta \frac{\Delta t}{2}\mathcal{J}^h E_{h\|}^n\left(\mathbf{r}_{h,j}^{\pm n}\right), \\ &\mathbf{r}_{h,j}^{\pm n+1/2} = \mathbf{r}_{h,j}^{\pm n} + \frac{\Delta t}{2} F_h^n\left(\mathbf{r}_{h,j}^{\pm n}, \mathcal{J}^h\phi_h^n, v_{h,j}^{\pm n}\right), \end{aligned} \tag{26}$$

where $\mathbf{r}_{h,j}^{\pm n+1/2} = \mathbf{r}_{\mathbf{k}} \in \mathcal{M}_h$, and

Step 2:

$$\begin{aligned} &v_{h,j}^{\pm n+1}\left(\mathbf{r}_{h,j}^{\pm n+1}\right) = v_{h,j}^{\pm n}\left(\mathbf{r}_{h,j}^{\pm n}\right) + Z_i\varepsilon_\delta \Delta t \mathcal{J}^h E_{h\|}^{n+1/2}\left(\mathbf{r}_{h,j}^{\pm n+1/2}\right), \\ &\mathbf{r}_{h,j}^{\pm n+1} = \mathbf{r}_{h,j}^{\pm n} + \Delta t F_h^{n+1/2}\left(\mathbf{r}_{h,j}^{\pm n+1/2}, \mathcal{J}^h\phi_h^{n+1/2}, v_{h,j}^{\pm n+1/2}\right), \end{aligned} \tag{27}$$

where $\mathbf{r}_{h,j}^{\pm n+1} = \mathbf{r}_{\mathbf{k}} \in \mathcal{M}_h$.

If we set $\mathbf{r}_{h,j}^{\pm n} = \mathbf{r}_{\mathbf{k}} - \mathbf{d}_{h,j}^{\pm n}$ in the recurrence equation (26) we are leaded to solve the fixed-point equation

$$\mathbf{d}_{h,j}^{\pm n} = \frac{\Delta t}{2} F_h^n\left(\mathbf{r}_{\mathbf{k}} - \mathbf{d}_{h,j}^{\pm n}, \mathcal{J}^h\phi_h^n, v_{h,j}^{\pm n}\right). \tag{28}$$

If we set $\mathbf{r}_{h,j}^{\pm n} = \mathbf{r}_{\mathbf{k}} - 2\mathbf{d}_{h,j}^{\pm n}$ in the recurrence equation (27) and make the approximation $\mathbf{r}_{h,j}^{\pm n+1/2} = \left(\mathbf{r}_{h,j}^{\pm n} + \mathbf{r}_{\mathbf{k}}\right)/2$, still valid at second order in time, we are leaded to solve the fixed-point equation

$$\mathbf{d}_{h,j}^{\pm n} = \frac{\Delta t}{2} F_h^{n+1/2}\left(\mathbf{r}_{\mathbf{k}} - \mathbf{d}_{h,j}^{\pm n}, \mathcal{J}^h\phi_h^{n+1/2}, v_{h,j}^{\pm n+1/2}\right). \tag{29}$$

Finally (28) and (29) are fixed-point problems of the form

$$\mathbf{d}_{\mathbf{k}} = \frac{\Delta t}{2} F_h\left(\mathbf{r}_{\mathbf{k}} - \mathbf{d}_{\mathbf{k}}, \mathcal{J}^h\phi_h, v_{h,j}^{\pm}\right). \tag{30}$$

The fixed-point problem (30) can be solved iteratively by a Newton algorithm. If we define the vector-valued function $\mathfrak{R}(\mathbf{d}_{\mathbf{k}}) = \mathbf{d}_{\mathbf{k}} - \frac{\Delta t}{2} F_h\left(\mathbf{r}_{\mathbf{k}} - \mathbf{d}_{\mathbf{k}}, \mathcal{J}^h\phi_h, v_{h,j}^{\pm}\right)$ a Newton iterate is given by

$$\mathbf{d}_{\mathbf{k}}^{\ell+1} = \mathbf{d}_{\mathbf{k}}^{\ell} - J_{\mathfrak{R}}^{-1}(\mathbf{d}_{\mathbf{k}}^{\ell})\mathfrak{R}(\mathbf{d}_{\mathbf{k}}^{\ell}), \tag{31}$$

where $J_{\mathfrak{R}}$ is the Jacobian matrix of $\mathfrak{R}$. Even if this algorithm gives accurate results, this method required interpolation of the fields $(\phi_h, v_{h,j}^{\pm})$ and its derivatives at arbitrary points of space. A less expensive solution is to Taylor-expand the iteration scheme (31) in time. Using the following second-order Taylor expansion of the inverse of the Jacobian matrix $J_{\mathfrak{R}}$,

$$J_{\mathfrak{R}}^{-1}(\mathbf{r}_{\mathbf{k}}) = \left(I + \frac{\Delta t}{2} J_{F_h}\left(\mathbf{r}_{\mathbf{k}} - \mathbf{d}_{\mathbf{k}}, \mathcal{J}^h\phi_h, v_{h,j}^{\pm}\right)\right)^{-1} = I - \frac{\Delta t}{2} J_{F_h}\left(\mathbf{r}_{\mathbf{k}} - \mathbf{d}_{\mathbf{k}}, \mathcal{J}^h\phi_h, v_{h,j}^{\pm}\right) + \mathcal{O}(\Delta t^2),$$

in Eq. (31) we get

$$\mathbf{d}_{\mathbf{k}}^{\ell+1} = \frac{\Delta t}{2} F_h\left(\mathbf{r}_{\mathbf{k}} - \mathbf{d}_{\mathbf{k}}^{\ell}, \mathcal{J}^h\phi_h, v_{h,j}^{\pm}\right) + \frac{\Delta t}{2} J_{F_h}\left(\mathbf{r}_{\mathbf{k}} - \mathbf{d}_{\mathbf{k}}^{\ell}, \mathcal{J}^h\phi_h, v_{h,j}^{\pm}\right)\left(\mathbf{d}_{\mathbf{k}}^{\ell} - \frac{\Delta t}{2} F_h\left(\mathbf{r}_{\mathbf{k}} - \mathbf{d}_{\mathbf{k}}^{\ell}, \mathcal{J}^h\phi_h, v_{h,j}^{\pm}\right)\right) + \mathcal{O}(\Delta t^2).$$

If we set the initial value $\mathbf{d}_{\mathbf{k}}^0$ to zero, then we get the simpler scheme

$$\mathbf{d}_{\mathbf{k}}^{\star} = \frac{\Delta t}{2} F_h\left(\mathbf{r}_{\mathbf{k}}, \mathcal{J}^h\phi_h, v_{h,j}^{\pm}\right) - \frac{\Delta t^2}{4} J_{F_h}\left(\mathbf{r}_{\mathbf{k}}, \mathcal{J}^h\phi_h, v_{h,j}^{\pm}\right) F_h\left(\mathbf{r}_{\mathbf{k}}, \mathcal{J}^h\phi_h, v_{h,j}^{\pm}\right) + \mathcal{O}(\Delta t^2), \tag{32}$$

which has the advantage to require the evaluation of F_h and its first derivatives only at the mesh nodes. If the we take $\mathbf{d}_{\mathbf{k}}^0$ in the Newton algorithm (31) and if it converges in one iteration, then it is equivalent to the method (32). Let us precise that we make a local two-dimensional Cartesian coordinates transform in the transversal direction to compute the characteristic origin. It now remains to solve the quasineutrality equation (12) and the gyroaverage operator (4) which are performed by spectral Fourier expansion in periodic directions and finite differences in the radial direction. If $\phi_{mn}(r)$ denotes the poloidal–toroidal mode (m,n) the Fourier transformed quasineutrality equation (12) becomes

$$-\frac{\zeta}{rn_{i0}(r)}\partial_r(rn_{i0}(r)\partial_r\phi_{mn}) + \left(\zeta\frac{m^2}{r^2} + \frac{\varepsilon_\delta\tau}{T_{i0}}(1-\lambda\delta_{m,0}\delta_{n,0})\right)\phi_{mn} = \rho_{mn} = \frac{1}{n_{i0}}\sum_{j=1}^{\mathcal{N}}\mathcal{A}_j((\mathcal{J}v_j^+)_{mn} - (\mathcal{J}v_j^-)_{mn}) - 1 \tag{33}$$

with $\zeta = \varepsilon_\delta\varepsilon_\omega^2\varepsilon_k^{-2}Z_i$. If we require that the electric field is uniquely defined and finite on the axis $r_{\min} = 0$, then the boundary conditions for the electrical potential must satisfied $\partial_r\phi_{0n}{}_{|r_{\min}=0} = 0,\ \forall n$ and $\phi_{mn}{}_{|r_{\min}=0} = 0,\ \forall m\neq 0,\ \forall n$. If $r_{\min}\neq 0$ we impose that $\phi_{mn}{}_{|r_{\min}=0} = 0,\ \forall(m,n)$. On the outer boundary the plasma is considered as a conductor, which means that there is no tangential electric field and thus $\phi_{mn}{}_{|r_{\max}=0} = 0,\ \forall(m,n)\neq 0$. In addition we impose $\phi_{00}{}_{|r_{\max}=0} = 0$. Using second-order finite differences Eq. (33) is recast in the $(N_r-1)\times(N_r-1)$ tridiagonal linear system

$$\begin{pmatrix} \varpi a+\alpha_1 & \beta_1^+ & & & \\ \beta_2^- & \alpha_2 & \beta_2^+ & 0 & \\ & \ddots & \ddots & \ddots & \\ & 0 & \beta_{N_r-2}^- & \alpha_{N_r-2} & \beta_{N_r-2}^+ \\ & & & \beta_{N_r-1}^- & \alpha_{N_r-1} \end{pmatrix} \begin{pmatrix} \phi_{mn,1} \\ \phi_{mn,2} \\ \vdots \\ \phi_{mn,N_r-2} \\ \phi_{mn,N_r-1} \end{pmatrix} = \begin{pmatrix} \rho_{mn,1} \\ \rho_{mn,2} \\ \vdots \\ \rho_{mn,N_r-2} \\ \rho_{mn,N_r-1} \end{pmatrix},$$

where

$$\alpha_i = \zeta\left(\frac{2}{\Delta r^2} + \frac{m^2}{r_i^2}\right) + \frac{\varepsilon_\delta\tau}{T_{i0}}(1-\lambda\delta_{m,0}\delta_{n,0}),$$
$$\beta_i^{\pm} = -\frac{\zeta}{\Delta r^2} \pm \frac{\zeta}{2\Delta r}\left(\frac{1}{r_i} + \frac{1}{n_{i0}(r_i)}\frac{dn_{i0}}{dr}(r_i)\right),$$
$$a = -\frac{\zeta}{\Delta r^2} + \frac{\zeta}{2\Delta r}\left(\frac{1}{r_1} + \frac{1}{n_{i0}(r_1)}\frac{dn_{i0}}{dr}(r_1)\right)$$

with $\varpi = 1$ if $r_{\min} = 0$ and $\varpi = 0$ if $r_{\min}\neq 0$. Let us note that in Eq. (33) the gyroaverage operator $\mathcal{J}$ (Eq. (4)) is replaced by its numerical approximation $\mathcal{J}^h$. It remains now to compute $\mathcal{J}^h$. In Fourier space the gyroaverage transform (4) becomes

$$-\frac{\rho^2}{4}\partial_r^2\langle\phi_{mn}\rangle + \left(1 - \frac{\rho^2}{4}\frac{m^2}{r^2}\right)\langle\phi_{mn}\rangle = \phi_{mn}, \tag{34}$$

where $\langle\phi_{mn}\rangle$ denotes the gyroaveraged potential poloidal–toroidal mode (m,n). Using a finite differences scheme and applying the same boundary conditions used for the quasineutrality equation, Eq. (34) leads to solve the tridiagonal linear system

$$\begin{pmatrix} \varpi\varrho+\gamma_1 & \varrho & & & \\ \varrho & \gamma_2 & \varrho & 0 & \\ & \ddots & \ddots & \ddots & \\ & 0 & \varrho & \gamma_{N_r-2} & \varrho \\ & & & \varrho & \gamma_{N_r-1} \end{pmatrix} \begin{pmatrix} \langle\phi_{mn,1}\rangle \\ \langle\phi_{mn,2}\rangle \\ \vdots \\ \langle\phi_{mn,N_r-2}\rangle \\ \langle\phi_{mn,N_r-1}\rangle \end{pmatrix} = \begin{pmatrix} \phi_{mn,1} \\ \phi_{mn,2} \\ \vdots \\ \phi_{mn,N_r-2} \\ \phi_{mn,N_r-1} \end{pmatrix},$$

where

$$\gamma_i = 1 + \frac{\rho^2}{4}\left(\frac{2}{\Delta r^2} + \frac{m^2}{r_i^2}\right), \quad \text{and} \quad \varrho = -\frac{\rho^2}{4\Delta r^2}.$$

Every tridiagonal linear system is solved by a LU factorization method.

4.2. Numerical approximation of the quasilinear system

This section is devoted to the numerical approximation of the system of Eqs. (19)–(22). To this aim we use the Runge–Kutta Discontinuous Galerkin method [12]. We first depict the method for the transport equations (19) and (20). Let be Ω the domain of computation and $\mathcal{M}_h$ a partition of Ω of element K such that $\cup_{K\in\mathcal{M}_h}\overline{K} = \overline{\Omega}$,

$K \cap Q = \emptyset,\ K, Q \in \mathcal{M}_h,\ K \neq Q$. We set $h = \max_{K \in \mathcal{M}_h} h_K$ where h_K is the exterior diameter of a finite element K. The boundary of K is denoted by ∂K, n_K is the outward unit normal to ∂K, and $f(\cdot) = (\cdot)^2/2$. Let us introduce the notations $V_{jm}^{\pm} = (\Re e V_{jm}^{\pm}, \Im m V_{jm}^{\pm})^T = (V_{jm}^{\pm 1}, V_{jm}^{\pm 2})^T$, $\gamma_\alpha = (-1)^\alpha$, and $\beta = \mathrm{mod}(\alpha, 2) + 1$. The first step of the method is to write Eqs. (19)–(22) in a variational (weak) form on any element K of the partition $\mathcal{M}_h$, i.e. we multiply (19)–(22) with a regular test-function and we integrate over the element K using a Green formula to make appear a boundary integral on the edge ∂K. We now seek an approximate solution $(v_{h,j0}^{\pm}, \Re e V_{h,jm}^{\pm}, \Im m V_{h,jm}^{\pm}, \phi_{h,0}, \Re e \Phi_{h,m}, \Im m \Phi_{h,m})$ whose restriction to the element K of the partition $\mathcal{M}_h$ of Ω belongs, for each value of the time variable, to the finite-dimensional local space $\mathcal{P}(K)$, typically a space of polynomials. We then set

$$\mathcal{P}_h(\Omega) = \{\psi \ |\psi_{|_K} \in \mathcal{P}(K),\ \forall K \in \mathcal{M}_h\}.$$

Therefore we determine the approximate solution $(v_{h,j0}^{\pm}, \Re e V_{h,jm}^{\pm}, \Im m V_{h,jm}^{\pm}, \phi_{h,0}, \Re e \Phi_{h,m}, \Im m \Phi_{h,m})_{|_K} \in \otimes^9 \mathcal{P}(K)$ for $t > 0$, on each element K of $\mathcal{M}_h$ by imposing that, for all $\varphi_h \in \mathcal{P}_h(\Omega)$, for all $j = 1, \ldots, \mathcal{N}$, for $\alpha \in \{1, 2\}$,

$$\begin{aligned}
&\partial_t \int_K dK\, v_{h,j0}^{\pm} \varphi_h - \frac{1}{2} \int_K dK \left(v_{h,j0}^{\pm}\right)^2 \partial_z \varphi_h + \int_{\partial K} d\Gamma \langle f n_{K,z} \rangle (v_{h,j0}^{\pm}) \varphi_h + Z_i \varepsilon_\delta \int_K dK \varphi_h E_{h,0z} \\
&\quad - \varepsilon_\delta \varepsilon_\omega \varepsilon_k^{-2} Z_i \sum_{m>0} m \left(\int_K dK V_{h,jm}^{\pm} \times \Phi_{h,m} \partial_r \left(\frac{\varphi_h}{2r}\right) - \int_{\partial K} d\Gamma \langle V_{h,jm}^{\pm} \times \Phi_{h,m} n_{K,r} \rangle \frac{\varphi_h}{2r} \right) \\
&\quad - \sum_{m>0} \left(\frac{1}{4} \int_K dK |V_{h,jm}^{\pm}|^2 \partial_z \varphi_h - \frac{1}{2} \int_{\partial K} d\Gamma \left(\langle f n_{K,z} \rangle (\Re e V_{h,jm}^{\pm}) + \langle f n_{K,z} \rangle (\Im m V_{h,jm}^{\pm}) \right) \varphi_h \right) \\
&\quad = 0
\end{aligned} \tag{35}$$

with

$$\int_K dK \varphi_h E_{h,0z} = -\int_K dK \phi_{h,0} \partial_z \varphi_h + \int_{\partial K} d\Gamma \langle \phi_{h,0} n_{K,z} \rangle \varphi_h \tag{36}$$

and

$$\begin{aligned}
&\partial_t \int_K dK V_{h,jm}^{\pm\alpha} \varphi_h + \varepsilon_\delta \varepsilon_\omega \varepsilon_k^{-2} Z_i \int_K dK \frac{\gamma_\alpha m}{r} \left(E_{h,0r} V_{h,jm}^{\pm\beta} - \partial_r v_{h,j0}^{\pm} \Phi_{h,m}^{\beta} \right) \varphi_h - \int_K dK\, v_{h,j0}^{\pm} V_{h,jm}^{\pm\alpha} \partial_z \varphi_h \\
&\quad + \int_{\partial K} d\Gamma \langle v_{h,j0}^{\pm} V_{h,jm}^{\pm\alpha} n_{K,z} \rangle \varphi_h + Z_i \varepsilon_\delta \int_K dK E_{h,mz}^{\alpha} \varphi_h \\
&\quad = 0,
\end{aligned} \tag{37}$$

where

$$\int_K dK \varphi_h E_{h,0r} = -\int_K dK \phi_{h,0} \partial_r \varphi_h + \int_{\partial K} d\Gamma \langle \phi_{h,0} n_{K,r} \rangle \varphi, \tag{38}$$

$$\int_K dK \partial_r v_{h,j0}^{\pm} \varphi_h = -\int_K dK\, v_{h,j0}^{\pm} \partial_r \varphi_h + \int_{\partial K} d\Gamma \langle v_{h,j0}^{\pm} n_{K,r} \rangle \varphi_h, \tag{39}$$

$$\int_K dK \varphi_h E_{h,mz}^{\alpha} = -\int_K dK \Phi_{h,m}^{\alpha} \partial_z \varphi_h + \int_{\partial K} d\Gamma \langle \Phi_{h,m}^{\alpha} n_{K,z} \rangle \varphi_h. \tag{40}$$

In Eqs. (35)–(40) we have replaced the flux terms at the boundary of the cell K, by numerical fluxes (bracket notation) because the terms arising from the boundary of the cell K are not well defined or have no sense since all unknowns are discontinuous (by construction of the space of approximation) on the boundary ∂K of the element K. Now it remains to define these numerical fluxes. For two adjacent cells K^ℓ and K^{r} (r denotes the right cell and ℓ the left one) of $\mathcal{M}_h$ and a point P of their common boundary at which the vector $n_{K^\sigma}, \sigma \in \{\mathrm{r}, \ell\}$ are defined, we set $\varphi_h^\sigma(P) = \lim_{\epsilon \to 0} \varphi_h(P - \epsilon n_{K^\sigma})$ and call these values the traces of φ_h from the interior of K^σ. Therefore the numerical flux at P is a function of the left and right traces of the unknowns considered. For example

$$\langle f n_{K^\ell,z} \rangle (v_{h,j0}^{\pm})(P) = \langle f n_{K^\ell,z} \rangle (v_{h,j0}^{\pm,\ell}(P), v_{h,j0}^{\pm,\mathrm{r}}(P)).$$

Besides the numerical flux must be consistent with the nonlinearity $f n_{K^\ell,z}$, which means that we should have $\langle f n_{K^\ell,z} \rangle (v, v) = f(v) n_{K^\ell,z}$. In order to give monotone scheme in case of piecewise-constant approximation the numerical flux must be conservative, i.e.

$$\langle f n_{K^\ell,z} \rangle (v_{h,j0}^{\pm,\ell}(P), v_{h,j0}^{\pm,\mathrm{r}}(P)) + \langle f n_{K^{\mathrm{r}},z} \rangle (v_{h,j0}^{\pm,\mathrm{r}}(P), v_{h,j0}^{\pm,\ell}(P)) = 0$$

and the mapping $v \mapsto \langle f n_{K^\ell,z} \rangle (v, \cdot)$ must be non-decreasing. There exist several examples of numerical fluxes satisfying the above requirements: the Godunov flux, the Engquist–Osher flux, the Lax–Friedrichs flux (see [12]). For the numerical fluxes $\langle V_{h,jm}^{\pm} \times \Phi_{h,m} n_{K,r} \rangle, \langle f n_{K,z} \rangle (\Re e V_{h,jm}^{\pm})$, and $\langle f n_{K,z} \rangle (\Im m V_{h,jm}^{\pm})$ we choose the average flux. For the fluxes $\langle \phi_{h,0} n_{K,z} \rangle, \langle \phi_{h,0} n_{K,r} \rangle, \langle v_{h,j0}^{\pm} n_{K,r} \rangle$ and $\langle \Phi_{h,m}^{\alpha} n_{K,z} \rangle$ we can choose the average, left or right flux. Finally for the numerical flux $\langle v_{h,j0}^{\pm} V_{h,jm}^{\pm\alpha} n_{K,z} \rangle$ (with discontinuous advection coefficient) we can choose two different upwind fluxes

$$\left\langle v^{\pm}_{h,j0} V^{\pm\alpha}_{h,jm} n_{K,z} \right\rangle = \left\langle v^{\pm}_{h,j0} n_{K,z} \right\rangle^{\triangle} V^{\pm\alpha,\ell}_{h,jm} + \left\langle v^{\pm}_{h,j0} n_{K,z} \right\rangle^{\triangledown} V^{\pm\alpha,\mathrm{r}}_{h,jm},$$

where

- $\langle v^{\pm}_{h,j0} n_{K,z}\rangle^{\triangle} = (v^{\pm,\ell}_{h,j0})^{\triangle} |n_{K,z}|$, $\langle v^{\pm}_{h,j0} n_{K,z}\rangle^{\triangledown} = (v^{\pm,\mathrm{r}}_{h,j0})^{\triangledown} |n_{K,z}|$
  or
- $\langle v^{\pm}_{h,j0} n_{K,z}\rangle = |n_{K,z}|((1-\eta) v^{\pm,\ell}_{h,j0} + \eta v^{\pm,\mathrm{r}}_{h,j0}), \quad \eta \in [0,1]$
  with the notation $z^{\triangle} = \max(z,0)$ and $z^{\triangledown} = \min(z,0)$.
  Let us introduce X_h, a generic unknown such that

$$X_h \in \Lambda = \left\{ \left\{ v^{\pm}_{h,j0} \right\}_{j\in[1,\mathcal{N}]}, \left\{ V^{\pm}_{h,jm} \right\}_{j\in[1,\mathcal{N}],m>0} \right\}.$$

Therefore, after the space-discretization step, for all $K \in \mathcal{M}_h$ and $X_h \in \Lambda$, we get the ordinary differential equations

$$\mathfrak{M} \frac{d}{dt} X_{h_{|K}} = \mathcal{L}_{K,X_h}\left(\left\{ v^{\pm}_{h,j0_{|K'}}, V^{\pm}_{h,jm_{|K'}}, \phi_{h,0_{|K'}}, \Phi_{h,m_{|K'}} \mid \overline{K'} \cap \overline{K} \in \partial K \right\} \right).$$

In the general case, the local mass matrix $\mathfrak{M}$ of low order (equal to the dimension of the local space $\mathcal{P}(K)$) is easily invertible. If we choose orthogonal polynomials the matrix $\mathfrak{M}$ is diagonal. Here we take Legendre polynomials as L^2-orthogonal basis function. Our code can run with Legendre polynomials of any degree, but for the numerical results exposed in the next section we choose polynoms of degree two. Moreover we take a rectangular element $K = K_{pq} = \{(r,z) || r_p - r| \leqslant \Delta r/2, |z_q - z| \leqslant \Delta z/2\}$, where Δr and Δz are the space-discretization parameters.

Therefore we have to solve the ordinary differential equations

$$\frac{d}{dt} X_h = L_{h,X_h}\left(v^{\pm}_{h,j0}, V^{\pm}_{h,jm}, \phi_{h,0}, \Phi_{h,m} \right), \quad \forall X_h \in \Lambda. \tag{41}$$

In order to solve ODE's (41) we can use Runge–Kutta methods [24]. For numerical stability considerations we have to choose $k+1$ stage Runge–Kutta method of order $k+1$ for DG discretizations using polynomials of degree k if we do not want our CFL number to be too small. Since we take polynomial of degree two we choose the third-order strong stability-preserving Runge–Kutta method [24]:

$$\begin{aligned}
X_h(t_1) &= X_h(t^n) + \Delta t L_{h,X_h}\left(v^{\pm}_{h,j0}(t^n), V^{\pm}_{h,jm}(t^n), \phi_{h,0}(t^n), \Phi_{h,m}(t^n) \right),\\
X_h(t_2) &= \frac{3}{4} X_h(t^n) + \frac{1}{4} X_h(t_1) + \frac{1}{4} \Delta t L_{h,X_h}\left(v^{\pm}_{h,j0}(t_1), V^{\pm}_{h,jm}(t_1), \phi_{h,0,}(t_1), \Phi_{h,m}(t_1) \right),\\
X_h(t^{n+1}) &= \frac{1}{3} X_h(t^n) + \frac{2}{3} X_h(t_2) + \frac{2}{3} \Delta t L_{h,X_h}\left(v^{\pm}_{h,j0}(t_2), V^{\pm}_{h,jm}(t_2), \phi_{h,0,}(t_2), \Phi_{h,m}(t_2) \right),
\end{aligned}$$

$\forall X_h \in \Lambda$ with $t^n = n\Delta T$, $\Delta t = T/N_T$, and t_1 and t_2 times between t^n and t^{n+1}.

For the discretization of the initial condition we take $(v^{\pm}_{h,j0}(t=0), V^{\pm}_{h,jm}(t=0))$ on the cell K to be the L^2-projection of $(v^{\pm}_{j0}(t=0), V^{\pm}_{jm}(t=0))$ on $\otimes^6 \mathcal{P}(K)$.

It now remains to solve the quasineutrality equations (21) and (22). If we set $\lambda = 0$, Eqs. (21) and (22) take the general form

$$\partial_r \sigma + \nu \phi = \rho \quad \text{on } \Omega, \tag{42}$$

$$\mu^{-1} \sigma = -\partial_r \phi \quad \text{on } \Omega, \tag{43}$$

$$\phi_{|r=r_{\min}} = 0 \text{ or } \partial_r \phi_{|r=r_{\min}} = 0, \quad \text{and} \quad \phi_{|r=r_{\max}} = 0, \ \forall z \in \Omega_z, \tag{44}$$

$$\phi(r,z) = \phi(r, z+L_z), \quad \forall r \in \Omega_r, \tag{45}$$

where $\Omega = \Omega_r \times \Omega_z = [r_{\min}, r_{\max}] \times [0, L_z]$. The term ρ/r stands for the right hand side of (21) or (22), $\mu(r) = \varepsilon_\delta \varepsilon_k^{-2} \varepsilon_\omega^2 Z_i r n_{i0}(r)$, and we define $\nu(r) = \varepsilon_\delta \tau r n_{i0}(r)/T_{i0}(r)$ for Eq. (21) or $\nu(r) = r\varepsilon_\delta \varepsilon_\omega^2 \varepsilon_k^{-2} Z_i m^2/r^2 + \varepsilon_\delta \tau r n_{i0}(r)/T_{i0}(r)$ for Eq. (22). Using Green formula we can rewrite the problem (42)–(45) in a variational (weak) form suitable for its numerical approximation which consists in finding $\sigma_h \in \mathcal{P}_h(\Omega)$ and $\phi_h \in \mathcal{P}_h(\Omega)$ such that for all $\varphi_h, \psi_h \in \mathcal{P}_h(\Omega)$, and for all $K \in \mathcal{M}_h$

$$\int_K \mu^{-1} \sigma_h \varphi_h dK = \int_K \phi_h \partial_r \varphi_h dK - \int_{\partial K} \widehat{\phi}_K \varphi_h n_{K^\ell,r} d\Gamma, \tag{46}$$

$$\int_K \sigma_h \partial_r \psi_h dK = \int_{\partial K} \widehat{\sigma}_K n_{K^\ell,r} \psi_h d\Gamma + \int_K \nu \phi_h \psi_h dK - \int_K \rho_h \psi_h dK, \tag{47}$$

where σ_h and ϕ_h are approximations of $\sigma = -\mu \partial_r \phi$ and ϕ respectively, and ρ_h stands for the approximation of ρ in $\mathcal{P}_h(\Omega)$. The numerical fluxes $\widehat{\sigma}_K$ and $\widehat{\phi}_K$ are approximations of $\sigma = -\mu \partial_r \phi$ and ϕ respectively, on the boundary of the cell K. If we set n the outward unit normal to $\partial\Omega$, $\mathcal{E}_h^\circ$ the set of interior edges of $\mathcal{M}_h$, $\mathcal{E}_h^\partial$ the set of boundary edges of $\mathcal{M}_h$ and if we use the notations $[\![\varphi_h]\!] = \varphi_h^{\mathrm{r}} n_{K^\ell,r} + \varphi_h^\ell n_{K^{\mathrm{r}},r}$ and $\{\varphi_h\} = \frac{1}{2}(\varphi_h^{\mathrm{r}} + \varphi_h^\ell)$, then for $\varphi, \psi \in \prod_{K\in\mathcal{M}_h} L^2(\partial K)$ we have

$$\sum_{K\in\mathcal{M}_h}\int_{\partial K}\psi_{K^\ell}\varphi_{K^\ell}n_{K^\ell,r}d\Gamma=\int_{\mathcal{E}_h^\circ}(\llbracket\psi\rrbracket\{\varphi\}+\llbracket\varphi\rrbracket\{\psi\})d\Gamma+\int_{\mathcal{E}_h^\partial}\psi\varphi n_r d\Gamma. \tag{48}$$

If we take $\varphi_h=\sigma_h$ in Eq. (46), $\psi_h=\phi_h$ in Eq. (47), summing over the cell K and using Eq. (48) we obtain

$$\mathcal{R}_h+\int_\Omega\mu^{-1}|\sigma_h|^2dK+\int_\Omega v|\phi_h|^2dK=\int_\Omega\rho_h\phi_h dK, \tag{49}$$

where

$$\mathcal{R}_h=\int_{\mathcal{E}_h^\circ}\Big(\{\widehat{\sigma}_h-\sigma_h\}\llbracket\phi_h\rrbracket+\{\widehat{\phi}_h-\phi_h\}\llbracket\sigma_h\rrbracket\Big)d\Gamma+\int_{\mathcal{E}_h^\partial}\Big(\phi_h(\widehat{\sigma}_h-\sigma_h)+\widehat{\phi}_h\sigma_h\Big)n_r d\Gamma. \tag{50}$$

Now let us choose the numerical fluxes as follows

$$\widehat{\sigma}_h=\{\sigma_h\}+\alpha_{11}\llbracket\phi_h\rrbracket+\alpha_{12}\llbracket\sigma_h\rrbracket,\quad \widehat{\phi}_h=\{\phi_h\}-\alpha_{11}\llbracket\phi_h\rrbracket+\alpha_{22}\llbracket\sigma_h\rrbracket\quad\text{on }\mathcal{E}_h^\circ, \tag{51}$$

$$\widehat{\sigma}_h=\sigma_h^\ell+\alpha_{11}\phi_h^\ell n_r,\quad \widehat{\phi}_h=0,\quad\text{on }\mathcal{E}_h^\partial\cap\Gamma_D, \tag{52}$$

$$\widehat{\sigma}_h=0,\quad \widehat{\phi}_h=\phi_h^\ell+\alpha_{22}\sigma_h^\ell n_r,\quad\text{on }\mathcal{E}_h^\partial\cap\Gamma_N, \tag{53}$$

where $\alpha_{11}>0,\alpha_{22}\geqslant 0,\alpha_{12}\in\mathbb{R}$, and Γ_D (resp. Γ_N) denotes the boundary edges subset of $\mathcal{E}_h^\partial$ where Dirichlet conditions (resp. Neumann) are applied. If we plug the numerical fluxes (51)–(53) into Eq. (50) we then get

$$\mathcal{R}_h=\int_{\mathcal{E}_h^\circ}(\alpha_{11}\llbracket\phi_h\rrbracket^2+\alpha_{22}\llbracket\sigma_h\rrbracket^2)d\Gamma+\int_{\mathcal{E}_h^\partial\cap\Gamma_D}\alpha_{11}|\phi_h|^2d\Gamma+\int_{\mathcal{E}_h^\partial\cap\Gamma_N}\alpha_{22}|\sigma_h|^2d\Gamma\geqslant 0.$$

If we set $\rho_h=0$ in Eq. (49), then we get $\llbracket\phi_h\rrbracket_{|\mathcal{E}_h^\circ}=0,\phi_{h|_{\Gamma_D}}=0,\sigma_h=0$ and $\phi_h=0$ since $\mu,v,\alpha_{11}>0$ and $\alpha_{22}\geqslant 0$. Therefore $\phi_h=0$ on $\overline{\Omega}$ and the approximate solution ϕ_h is well defined. Now that the method supplies a unique approximate solution, let us compute it. If we take Eq. (46), sum over the cell K, by using the expression (48) we get

$$a(\sigma_h,\varphi_h)-b(\phi_h,\varphi_h)=0,\quad\forall\varphi_h\in\mathcal{P}_h(\Omega), \tag{54}$$

where the bilinear forms $a(\cdot,\cdot)$ and $b(\cdot,\cdot)$ are defined by

$$a(u,v)=\int_\Omega\mu^{-1}uvdK+\alpha_{22}\left(\int_{\mathcal{E}_h^\circ}\llbracket u\rrbracket\llbracket v\rrbracket d\Gamma+\int_{\mathcal{E}_h^\partial\cap\Gamma_N}(un_r)(vn_r)\right),$$

$$b(w,u)=\int_\Omega\partial_r uwdK+\int_{\mathcal{E}_h^\circ}\llbracket u\rrbracket(\alpha_{12}\llbracket w\rrbracket-\{w\})d\Gamma-\int_{\mathcal{E}_h^\partial\cap\Gamma_N}un_r w.$$

Using integration by part we get

$$-\int_K\sigma_h\partial_r\varphi_h dK=-\int_{\partial K}\sigma_h n_{K^\ell,r}\varphi_h d\Gamma+\int_K\partial_r\sigma_h\varphi_h dK. \tag{55}$$

If we add Eq. (47) to Eq. (55), sum over all cell K, and use Eq. (48) then, we get

$$b(\psi_h,\sigma_h)+c(\psi_h,\phi_h)=F(\psi_h),\quad\forall\psi_h\in\mathcal{P}_h(\Omega), \tag{56}$$

where the bilinear form $c(\cdot,\cdot)$ and the linear form $F(\cdot)$ are defined by

$$c(w,p)=\alpha_{11}\int_{\mathcal{E}_h^\circ}\llbracket w\rrbracket\llbracket p\rrbracket d\Gamma+\alpha_{11}\int_{\mathcal{E}_h^\partial}pwd\Gamma+\int_\Omega vpwdK,\quad F(w)=\int_\Omega w\rho_h dK.$$

The variational formulation (54)–(56), leads to the matrix formulation

$$\Xi_h^T\mathcal{A}\Sigma_h-\Phi_h^T\mathcal{B}\Psi_h=0,\quad\Psi_h^T\mathcal{B}\Sigma_h-\Psi_h^T\mathcal{C}\Phi_h=\Psi_h^TF_h,\quad\forall\Psi_h,\Xi_h,$$

which is equivalent to solve the linear system

$$\Sigma_h=\mathcal{A}^{-1}\mathcal{B}^T\Phi_h,\quad(\mathcal{B}\mathcal{A}^{-1}\mathcal{B}^T+\mathcal{C})\Phi_h=F_h. \tag{57}$$

We can solve the linear systems (57) by direct (LU decomposition for example) or iterative methods (conjugate gradient for example) of linear algebra. Let us note that if $\alpha_{22}=0$, then the matrix $\mathcal{A}$ is diagonal by block, and therefore it is easier to invert.

Remark 1. Up to this point we have assumed that all integrals involved in the definition of the numerical schemes are evaluated analytically. In fact all integrals can be reduced to the computation

$$\int_{-1}^1 f(\xi)d\xi. \tag{58}$$

To evaluate integral (58) we use numerical integration or quadrature rules whose the concept is the approximation of the integral by finite summation of the form

$$\int_{-1}^{1} f(\xi)d\xi \approx \sum_{i=0}^{Q-1} \omega_i f(\xi_i),$$

where ω_i are specified constants or weights and ξ_i represent an abscissa of Q distinct points in the interval $-1 \leqslant \xi_i \leqslant 1$. There are many types of numerical integration [30], here we choose Gaussian quadrature rules. In order to keep high-order accuracy, the quadrature rules should be exact for polynomial of degree $2k+1$ on ∂K and $2k$ on K where k is the degree of polynomial approximation [12].

5. Numerical results

5.1. Construction of a gyro-water-bag equilibrium

The first problem is to determine physically relevant gyro-water-bag equilibrium which will be use to initialize the numerical scheme depicted previously. In order to describe ITG modes, we choose to construct radial profiles in terms of temperature and density profiles only. The continuous equilibrium distribution function is assumed as

$$f_{eq}(r, v_\parallel) = \frac{n_{i0}(r)}{\sqrt{T_{i0}(r)}} \mathcal{F}\left(\frac{v_\parallel}{\sqrt{T_{i0}(r)}}\right), \tag{59}$$

where $n_{i0}(r)$ and $T_{i0}(r)$ are the normalized radial profiles of ion density and temperature. The function $\mathcal{F}$ is a normalized even function, thus for a local Maxwellian distribution, we get $\mathcal{F}(x) = \exp(-x^2/2)/\sqrt{2\pi}$. The first stage, will consist in constructing the gyro-water-bag equilibrium function at $r = r_0$, and then extended it for all $r \in [r_{\min}, r_{\max}]$. To this aim, as in [35], we use the method of equivalence between the radial derivatives of the moments of the stepwise gyro-water-bag function and the radial derivatives of the corresponding continuous function. If we define, for $\ell = 0, 2, \ldots, 2(\mathcal{N}-1)$, the r-derivative of the ℓ-moment of f_{eq} as

$$\mathcal{M}_r^\ell(f_{eq}) = \int_{\mathbb{R}} dv_\parallel \partial_r f_{eq} v_\parallel^\ell$$

and the r-derivative of the ℓ-moment of the gyro-water-bag as

$$\mathcal{M}_r^\ell(GWB) = \sum_j^{\mathcal{N}} 2\mathcal{A}_j v_j^{\circ\ell} \partial_r v_j^\circ,$$

then, using integration by parts, the equality $\mathcal{M}_r^\ell(f_{eq}) = \mathcal{M}_r^\ell(GWB)$ at the point $r = r_0$ implies

$$\sum_j^{\mathcal{N}} \alpha_j(r_0)\Omega^\star_{v_j^\circ}(r_0)(v_j^\circ(r_0))^\ell = \left(\Omega^\star_{n_{i0}}(r_0) + \frac{\ell}{2}\Omega^\star_{T_{i0}}(r_0)\right)\left(\sqrt{T_{i0}(r_0)}\right)^\ell \mathcal{M}^\ell(\mathcal{F}), \tag{60}$$

where $\mathcal{M}^\ell(\mathcal{F})$ is the ℓth order moment of the function $\mathcal{F}$, $\alpha_j = 2v_j^\circ \mathcal{A}_j / n_{i0}$, $\Omega^\star_{v_j^\circ}$ measuring the local radial gradient of the bag v_j°, $\Omega^\star_{n_{i0}}$ and $\Omega^\star_{T_{i0}}$ are the diamagnetic frequencies defined by

$$\Omega^\star_{v_j^\circ} = \frac{k_\theta T_{i0}}{q_i B}\frac{d\ln v_j^\circ}{dr} = \frac{k_\theta T_{i0}}{q_i B}\kappa_{v_j^\circ}$$

and

$$\Omega^\star_{n_{i0}} = \frac{k_\theta T_{i0}}{q_i B}\frac{d\ln n_{i0}}{dr} = \frac{k_\theta T_{i0}}{q_i B}\kappa_{n_{i0}}, \quad \Omega^\star_{T_{i0}} = \frac{k_\theta T_{i0}}{q_i B}\frac{d\ln T_{i0}}{dr} = \frac{k_\theta T_{i0}}{q_i B}\kappa_{T_{i0}}.$$

We now introduce the unknown coefficients β_j and γ_j, for $j = 1, \ldots, \mathcal{N}$, such that the constraint

$$\alpha_j \Omega_{v_j^\circ} = \gamma_j \Omega^\star_{n_{i0}} + \frac{1}{2}\beta_j \Omega^\star_{T_{i0}} \tag{61}$$

is satisfied at the point $r = r_0$. If we substitute (61) into (60) then, the unknown gyro-water-bag parameters $(\alpha_j, \beta_j, \gamma_j)$ must solve the following linear system at the point $r = r_0$,

$$\sum_{1\leqslant j\leqslant\mathcal{N}} \alpha_j(r_0)(v_j^\circ(r_0))^\ell = (\ell+1)\left(\sqrt{T_{i0}(r_0)}\right)^\ell \mathcal{M}^\ell(\mathcal{F}), \tag{62}$$

$$\sum_{1\leqslant j\leqslant\mathcal{N}} \beta_j(r_0)(v_j^\circ(r_0))^\ell = \ell\left(\sqrt{T_{i0}(r_0)}\right)^\ell \mathcal{M}^\ell(\mathcal{F}), \tag{63}$$

$$\sum_{1\leqslant j\leqslant\mathcal{N}} \gamma_j(r_0)(v_j^\circ(r_0))^\ell = \left(\sqrt{T_{i0}(r_0)}\right)^\ell \mathcal{M}^\ell(\mathcal{F}). \tag{64}$$

Nevertheless in Eqs. (62)–(64) the matrix has the form of a Vandermonde system which becomes ill-conditioned for a great number of bags $\mathcal{N}$. A more convenient solution can be found for a large number of bag. Let us consider a regular sampling of the $v_\parallel$-axis, i.e. $v_j^\circ(r_0) = (j-\frac{1}{2})\Delta v$, with $\Delta v = 2v_{\max}/(2\mathcal{N}-1)$ and set $F_j = f_{eq}(r_0, v_j^\circ(r_0) - \frac{\Delta v}{2})$. If we required that Eqs. (62)–(64) are satisfied at second order in Δv, then, using a trapeze quadrature rule to compute $\mathcal{M}^\ell(\mathcal{F})$, we get the solution

$$\alpha_j(r_0) = 2\mathcal{A}_j \frac{v_j^\circ(r_0)}{n_{i0}(r_0)} = 2(F_j - F_{j+1})\frac{v_j^\circ(r_0)}{n_{i0}(r_0)}, \quad \gamma_j(r_0) = \Delta v \frac{F_j + F_{j+1}}{n_{i0}(r_0)}, \quad \beta_j(r_0) = \alpha_j(r_0) - \gamma_j(r_0).$$

After defining a local equilibrium at $r = r_0$ by the method of moments equivalence, we extend the equilibrium in the radial direction by following the level lines of the continuous equilibrium (59) where the reference (boundary) level values are given by the equilibrium ones defined at $r = r_0$. Therefore gyro-water-bag parameters $\{\mathcal{A}_j\}_{j\in[1,\mathcal{N}]}$, and the initial condition for the quasilinear (QL) and nonlinear (NL) problem, for $j = 1,\dots,\mathcal{N}$, are given by

$$\begin{aligned}
&\mathcal{A}_j = F_j - F_{j+1},\\
&v_j^\circ(r) = \sqrt{T_{i0}(r)}\mathcal{F}^{-1}\left(f_j\frac{\sqrt{T_{i0}(r)}}{n_{i0}(r)}\right), \qquad (65)\\
&v_{j0}^\pm(0,r,z) = \pm v_j^\circ(r) \quad (\mathrm{QL}),\\
&v_j^\pm(0,r,\theta,z) = \pm v_j^\circ(r) \quad (\mathrm{NL}) \qquad (66)
\end{aligned}$$

with $f_j = f_{eq}(r_0, v_j^\circ(r_0))$. If we now differentiate (65) with respect to r, with $\mathcal{F}$ a normalized Maxwellian, we get

$$\kappa_{v_j^\circ}(r) = \frac{1}{2}\kappa_{T_{i0}}(r)\left(1 - \frac{T_{i0}(r)}{v_j^{\circ 2}(r)}\right) + \frac{T_{i0}(r)}{v_j^{\circ 2}(r)}\kappa_{n_{i0}}(r),$$

which says that

$$\kappa_{v_j^\circ} \sim \mathcal{O}\left(\kappa_T, \kappa_n, \frac{1}{v_j^{\circ 2}}\right)$$

and thus numerical problems could appear. In fact, if we keep a uniform $v_\parallel$-discretization to determine the gyro-water-bag equilibrium and if we want to use a large number of bag we see that $\kappa_{v_1^\circ}$ can explose as the first bag tends to zero. This phenomenon can lead to the bag crossing. In the same way, let us suppose that the number of bag remains fixed and the temperature gradient (resp. the density gradient) is homogeneous and fixed. If the density (resp. the temperature) varies to much in the radial direction then the equilibrium bags can cross each other.

The radial profiles of the ion density and temperature are fixed in time and are deduced by integration of their gradient profiles

$$\begin{aligned}
\kappa_{n_{i0}}(r) &= \frac{1}{n_{i0}(r)}\frac{dn_{i0}(r)}{dr} = -\kappa_{n_{i0}}^\circ \cosh^{-2}\left(\frac{r-r_0}{\Delta r_{n_{i0}}}\right),\\
\kappa_{T_{i0}}(r) &= \frac{1}{T_{i0}(r)}\frac{dT_{i0}(r)}{dr} = -\kappa_{T_{i0}}^\circ \cosh^{-2}\left(\frac{r-r_0}{\Delta r_{T_{i0}}}\right),
\end{aligned}$$

where $r_0, \kappa_{n_{i0}}^\circ, \kappa_{T_{i0}}^\circ, \Delta r_{n_{i0}}$ and $\Delta r_{T_{i0}}$ are free parameters. We next define the parameter $\eta(r) = d(\ln T_{i0})/d(\ln n_{i0})$ which determines locally if an ITG instability can develop ($\eta \geqslant 2$) or not ($\eta < 2$). The initial perturbation bag is chosen as

$$V_{jm}^\pm(0,r,z) = v_{j0}^\pm(0,r,z)p(r)\delta p(z) \quad (\mathrm{QL}), \quad \delta v_j^\pm(0,r,\theta,z) = v_j^\pm(0,r,\theta,z)p(r)\delta p(\theta,z) \quad (\mathrm{NL})$$

where $p(r)$ is an even exponential function centered in r_0 such that $\lim_{r\to r_{\min}} p(r) = 0$ and $\lim_{r\to r_{\max}} p(r) = 0$. The perturbation δp is initialized with a single mode or with a bath of modes

$$\begin{aligned}
\delta p(z) &= \sum_n \epsilon_n \cos\left(\frac{2\pi n}{L_z}z + \varphi_n\right) \quad (\mathrm{QL}),\\
\delta p(\theta,z) &= \sum_{nm} \epsilon_{nm} \cos\left(\frac{2\pi n}{L_z}z + m\theta + \varphi_{mn}\right) \quad (\mathrm{NL}),
\end{aligned}$$

where ϵ and φ represent respectively a random amplitude and a random phase for the mode considered.

5.2. ITG instability and gyrokinetic turbulence in a cylinder

The ITG instabilities correspond to small scale instabilities which start in the region where local temperature gradient exceeds local density gradient by some amount. Due to the existence of energy invariants in the system, the perturbated modes can not grow unbounded and after a linear phase of exponential increase, a local quasilinear saturation takes place leading to flattening of the local temperature profile. In the nonlinear phase, the existence of broad wave spectrum involving

mode coupling phenomena and nonlinear resonant wave–particle interaction leads to a state of developed plasma turbulence and to the appearance of anomalous heat transport.

Fig. 1 illustrates some examples of initial radial profiles that we consider for ion density, temperature and η-parameter at equilibrium. In order to compare numerical results to analytical ones and thus to validate the numerical approximation, we consider the case where in Eqs. (21), (22) and (12) there is neither polarization drift, nor gyroaverage operator, i.e. the second-order differential operator in the transverse direction is removed. In that case a linear analysis can be performed (see [35,36]), resulting in algebraic dispersion relation, local in the radial direction, which can be then rigorously solved, giving rise to analytical growth rate for the ITG instability. In this test case we set $\varepsilon_\omega = \varepsilon_k = \varepsilon_\delta = 10^{-3}$ and the radial domain is taken such as $r \in [1,5]$. As Vlasov codes, the advantage of our numerical approximation is that the perturbation can be initialized with a single mode (m,n). Therefore we select only one perturbative toroidal–poloidal mode such that $(m,n) = (20,1)$. The results are summarized in Table 1.

In spite of good agreement between numerical and theoretical linear growth rate values (Table 1), the QL and NL models are not well posed without polarization drift or gyroaverage operator and then they have no sense in the nonlinear regime because there is no differential operator in the transverse direction or physical mechanism which prevent the excitation of small scales without damping. In other words all the modes in the limit $k_\perp \to \infty$ are unstables which means that the solution blows up in a finite time. Therefore the next step is to compare the linear growth rate of ITG instability given by the quasi-linear model (19)–(22) – referred to QL – solved by a Runge–Kutta discontinuous Galerkin method and the nonlinear model (11) and (12) – referred to NL – solved by a Runge–Kutta semi-Lagrangian method. Even if the QL and the NL models are different they should have the same behaviour (more precisely the same growth rate for the ITG instability) in the linear regime. For this test case we choose a radial domain such as $r \in [1,9]$, and $z, \theta \in [0, 2\pi]$. The dimensionless parameters $\varepsilon_\omega, \varepsilon_k$ and ε_δ are set to 10^{-3} and the number of bag is fixed to $\mathcal{N} = 6$. The results are summarized in Table 2.

From Table 2 we observe that the QL and the NL models give the same ITG instability growth rate in the linear regime, which participates to the validation of the numerical approximation.

We now want to compare the level of the turbulence between the QL and the NL models. To this purpose we consider two test cases and show the time evolution of the electric energy and the turbulent heat flux. The discretization parameters of the two benchmarks are summarized in Tables 3 and 4. For both test cases we take the following parameter values $\tau = 1, \varepsilon_\omega = \varepsilon_k = \varepsilon_\delta = 10^{-3}, v_{\max} = 5, r_{\min} = 1, r_{\max} = 9, z, \theta \in [0, 2\pi]$ and $\mathcal{N} = 6$.

Fig. 2 shows the evolution of the logarithm of L^2-norm of the electrical potential at $r = r_0$ for the QL and NL models, while Fig. 3 depicts the corresponding mean heat flux at $r = r_0$. If in the linear stage the QL and NL models give the same results in term of growth rate, potential energy and mean heat flux, we observe that in the nonlinear regime their behaviour differ, as it is expected. We notice that the level of the L^2-norm of the electrical potential and the mean heat flux are always a little greater for the QL model that the NL one at the beginning of the nonlinear saturation phase. This remark can be explained by the fact that in the QL model most of nonlinear coupling are removed and thus the saturation regime occurs with a time delay

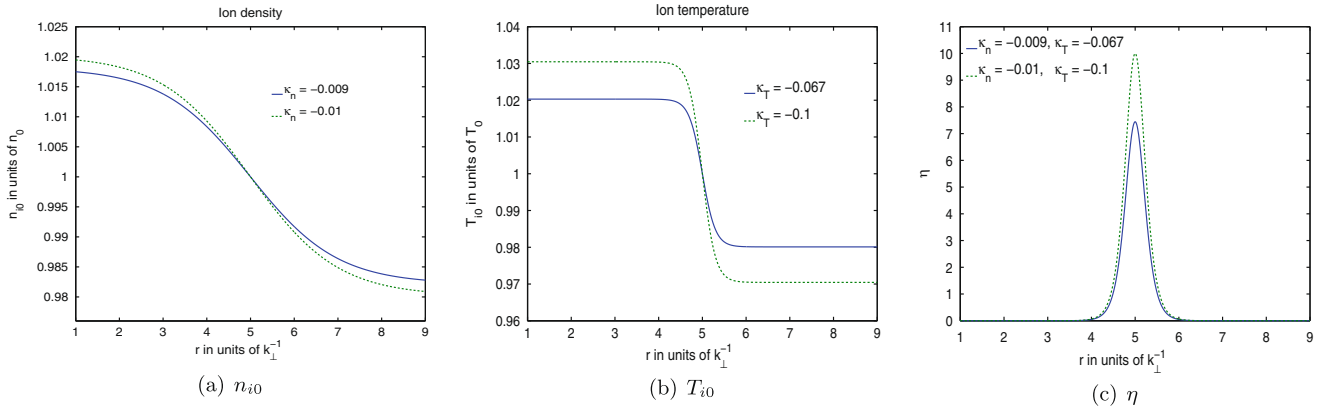

Fig. 1. Initial ion radial profiles: (a) density, (b) temperature, (c) η-parameter.

Table 1
Comparison of analytical and numerical growth rates in case of no polarization drift and no gyroaverage operator.

Case	$\kappa_n = 1.5 \times 10^{-4}$ $\kappa_T = 1.5 \times 10^{-3}$ $\mathcal{N} = 8, \tau = 1$ $v_{\max} = 6$	$\kappa_n = 1.5 \times 10^{-4}$ $\kappa_T = 1.5 \times 10^{-3}$ $\mathcal{N} = 10, \tau = 0.2$ $v_{\max} = 5$	$\kappa_n = 1.5 \times 10^{-4}$ $\kappa_T = 7.5 \times 10^{-4}$ $\mathcal{N} = 10, \tau = 1$ $v_{\max} = 5$	$\kappa_n = 1.5 \times 10^{-4}$ $\kappa_T = 6.45 \times 10^{-4}$ $\mathcal{N} = 10, \tau = 1$ $v_{\max} = 5$
γ_{theory}	0.80	1.80	0.22	0.097
γ_{numeric}	0.85	1.83	0.22	0.095

Table 2
Comparison of QL and NL growth rates.

Case	$\kappa_n = -0.02$ $\kappa_T = -0.1625$ $(m,n) = (6,3)$	$\kappa_n = -0.03$ $\kappa_T = -0.24$ $(m,n) = (6,3)$	$\kappa_n = -0.04$ $\kappa_T = -0.32$ $(m,n) = (6,3)$	$\kappa_n = -0.02$ $\kappa_T = -0.40$ $(m,n) = (6,3)$
γ_{QL}	1.70	2.12	2.44	4.30
γ_{NL}	1.70	2.12	2.44	4.30
	$\kappa_n = -0.01$ $\kappa_T = -0.08$ $(m,n) = (6,3)$	$\kappa_n = -0.01$ $\kappa_T = -0.075$ $(m,n) = (6,3)$	$\kappa_n = -0.009$ $\kappa_T = -0.069$ $(m,n) = (10,3)$	$\kappa_n = -0.009$ $\kappa_T = -0.067$ $(m,n) = (10,3)$
γ_{QL}	0.74	0.56	0.65	0.568
γ_{NL}	0.74	0.56	0.65	0.568

Table 3
Discretization parameters for the QL model.

	Δt	Δr	Δz	N_r	N_z	(m,n)
$\kappa_n = -0.009$ $\kappa_T = -0.067$	4×10^{-3}	1.25×10^{-1}	9.80×10^{-3}	64	64	$(10,3)$
$\kappa_n = -0.01$ $\kappa_T = -0.1$	4×10^{-3}	1.25×10^{-1}	9.80×10^{-3}	64	64	$(6,3)$

Table 4
Discretization parameters for the NL model.

	Δt	Δr	Δz	$\Delta\theta$	N_r	N_z	N_θ	(m,n)
$\kappa_n = -0.009$ $\kappa_T = -0.067$	4×10^{-3}	6.30×10^{-2}	4.90×10^{-2}	2.45×10^{-2}	128	128	256	$(10,3)$
$\kappa_n = -0.01$ $\kappa_T = -0.1$	7.85×10^{-3}	6.30×10^{-2}	9.80×10^{-2}	4.90×10^{-2}	128	64	128	$(6,3)$

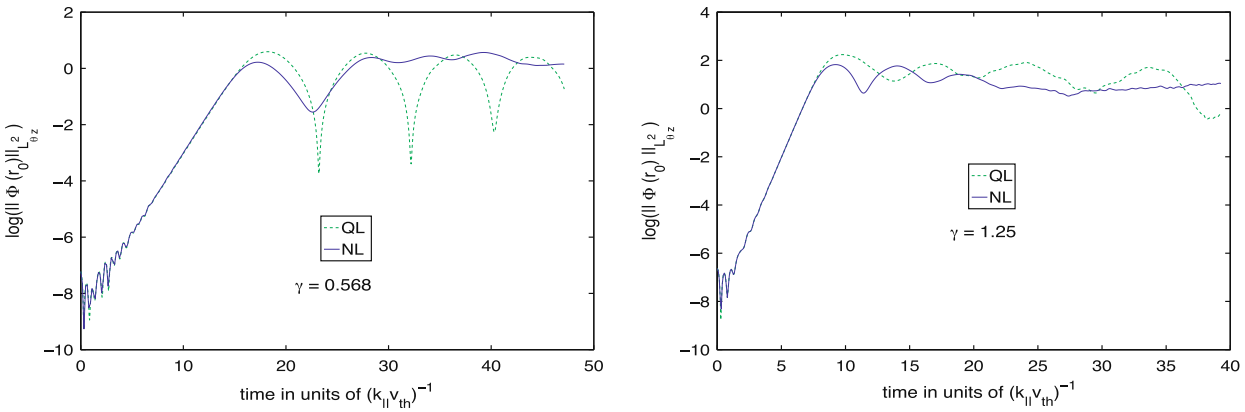

(a) $\kappa_n = -0.009$, $\kappa_T = -0.067$ (b) $\kappa_n = -0.01$, $\kappa_T = -0.1$

Fig. 2. L^2-norm of the electrical potential at $r = r_0$.

and an additional amount of electrical energy. Even if in the nonlinear regime QL and NL solutions are different, they remain qualitatively at the same level. Therefore the QL model constitutes a relative good approximation of the NL model even in the nonlinear phase.

If one wants to validate the nonlinear regime then it is always a problem because exact solutions are mostly not known. Nevertheless in our case, it is well known that the Vlasov equation conserves many physical and mathematical quantities such that mass, kinetic entropy, total energy, every L^p-norm, and more generally any phase-space integral of $\beta(f)$ where β

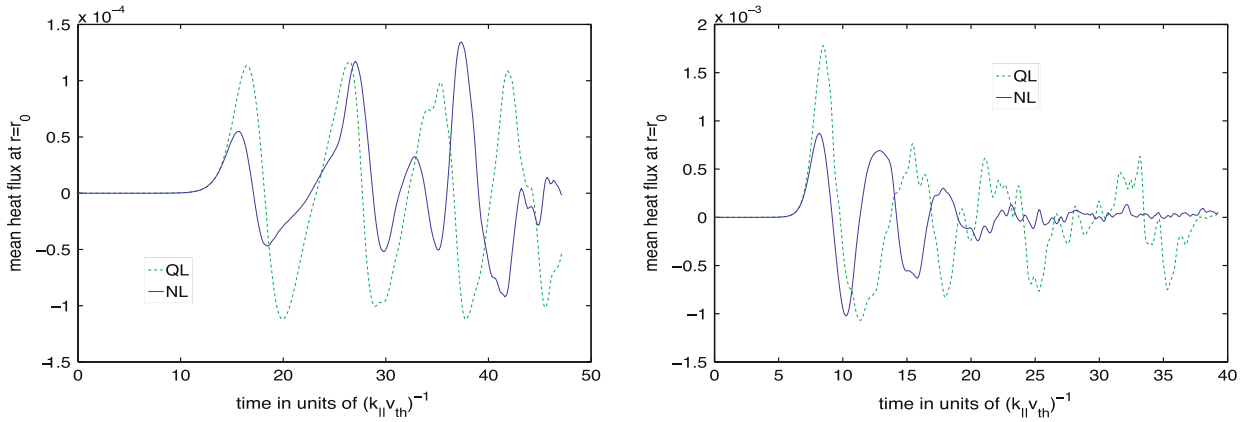

(a) $\kappa_n = -0.009$, $\kappa_T = -0.067$ (b) $\kappa_n = -0.01$, $\kappa_T = -0.1$

Fig. 3. Mean heat flux at $r = r_0$.

is a regular function. Obviously this conservation properties are retrieved with the gyro-water-bag model by using the distribution function (7). As a result, the usual integral Casimir invariants of the Vlasov equation become

$$\int \beta(f) 2\pi \frac{\Omega_i}{q_i} d\mathbf{r} dv_\parallel d\mu = \sum_{\mu j} 2\pi \frac{\Omega_i}{q_i} (\beta(f_{\mu j}) - \beta(f_{\mu j+1})) \int \left(v^+_{\mu j} - v^-_{\mu j} \right) d\mathbf{r}.$$

We next define the relative error Rel.Err.$(\mathcal{Q})$ of the conserved quantity $\mathcal{Q}$ as

$$\text{Rel.Err.}(\mathcal{Q})(t) = \frac{\mathcal{Q}(t) - \mathcal{Q}(0)}{\mathcal{Q}(0)}.$$

These invariants constitute good criteria to evaluate the behaviour of the numerical method in nonlinear stage. Fig. 4 shows the evolution of Rel.Err.$(\|f\|_{L^1})$, while Fig. 5 represents Rel.Err.$(\|f\|_{L^2})$. Finally Fig. 6 depicts the time evolution of Rel.Err.$(f \ln f)$. For the QL model, in the case corresponding to $\kappa_n = -0.009$ and $\kappa_T = -0.067$ the relative error of the L^2-norm, L^1-norm (or mass) and kinetic entropy is less than 10^{-12} and for the case where the radial gradients are $\kappa_n = -0.01$ and $\kappa_T = -0.1$, their relative errors remain below 10^{-9}. We notice that these conservations are better than those obtained for the NL model in the nonlinear regime. These results can be explained by the fact that growing small scale poloidal structures whose the size is smaller than the cell size are smoothed and then information is irreversibly lost resulting in deviation for every conserved quantity. Let us notice that in the NL model all poloidal modes, bounded by the mesh discretization in θ, can participate to the nonlinear regime by coupling to each other, whereas in the QL model they are fixed a priori ($m = 10$ or $m = 6$, in our case). Nevertheless even for the NL model the relative errors always stay less than 10^{-4}.

The conservation of energy is most difficult to satisfy as in PIC codes [28] or Vlasov codes [25]. In term of energy conservation the NL model behaves better than the QL one. In the light of the quasilinear analysis performed in [8], we know that the total energy is conserved at second order in the perturbation, thus it explains why energy conservation is less good in the case of the QL model. However this conservation is still correct even quite good since the relative error always remains below 3×10^{-4} for $\kappa_n = -0.009/\kappa_T = -0.067$ and below 5×10^{-3} for $\kappa_n = -0.01/\kappa_T = -0.1$ (see Fig. 7).

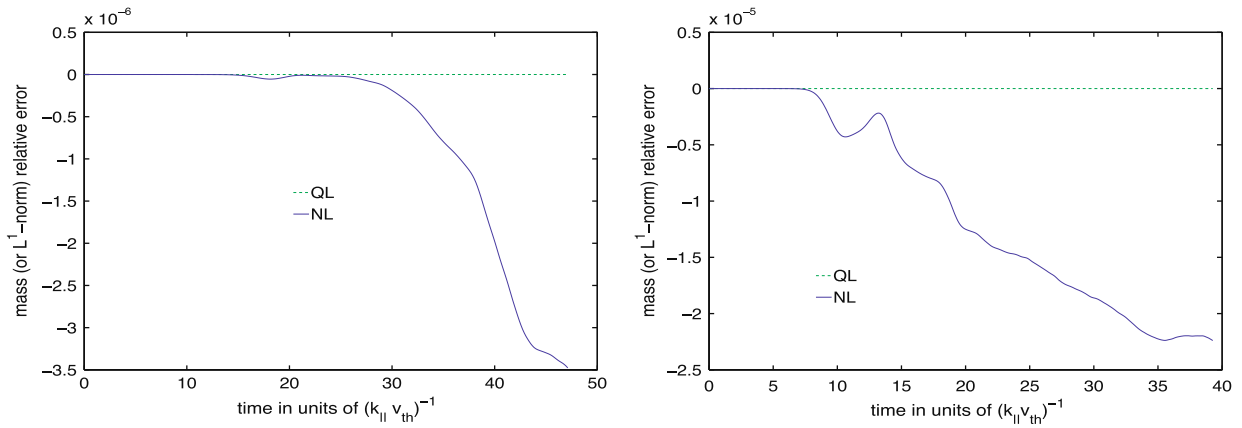

(a) $\kappa_n = -0.009$, $\kappa_T = -0.067$ (b) $\kappa_n = -0.01$, $\kappa_T = -0.1$

Fig. 4. Relative error on the L^1-norm (or mass) of f.

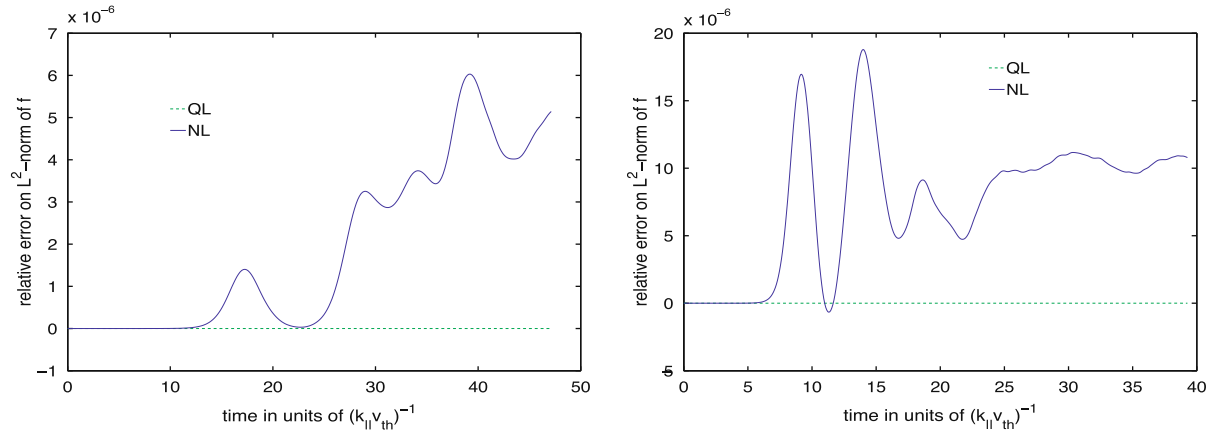

(a) $\kappa_n = -0.009$, $\kappa_T = -0.067$ (b) $\kappa_n = -0.01$, $\kappa_T = -0.1$

Fig. 5. Relative error on the L^2-norm of f.

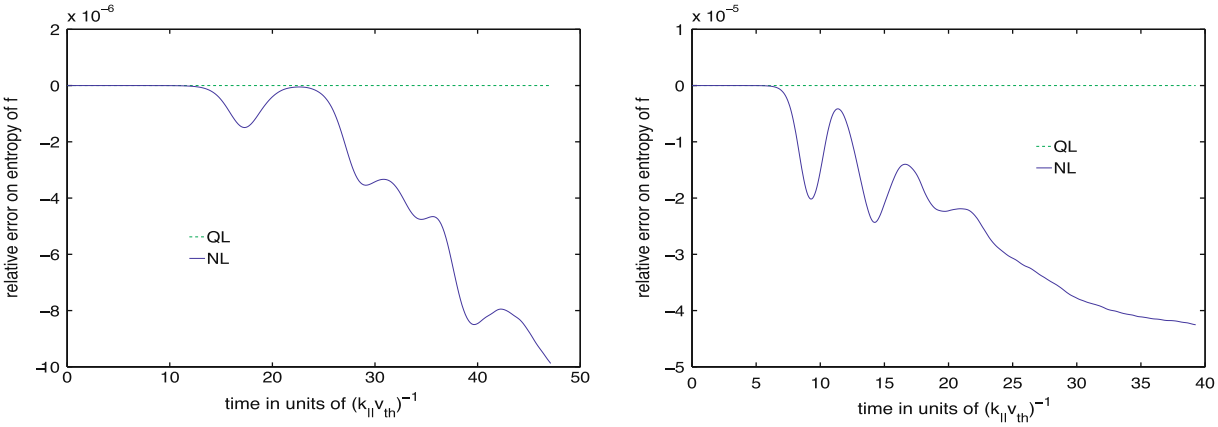

(a) $\kappa_n = -0.009$, $\kappa_T = -0.067$ (b) $\kappa_n = -0.01$, $\kappa_T = -0.1$

Fig. 6. Relative error on the entropy of f.

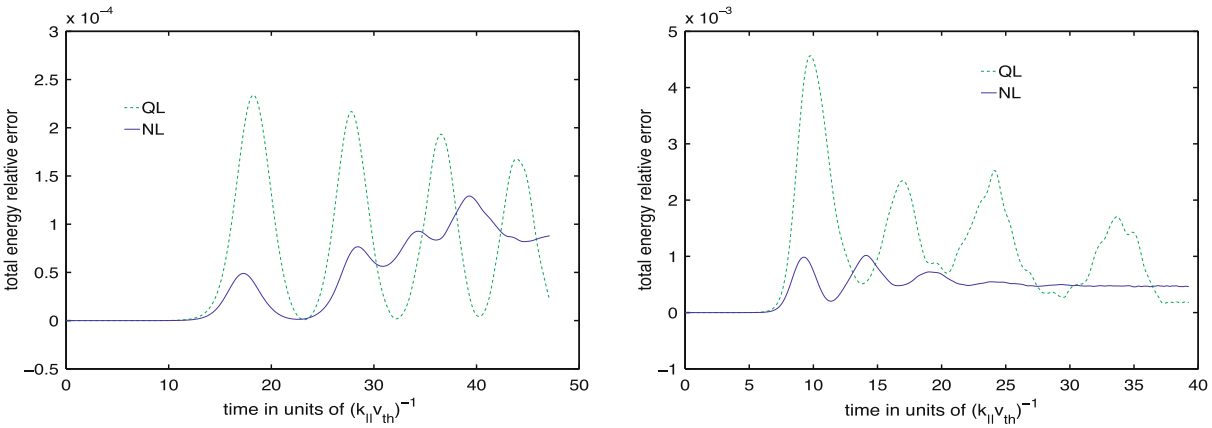

(a) $\kappa_n = -0.009$, $\kappa_T = -0.067$ (b) $\kappa_n = -0.01$, $\kappa_T = -0.1$

Fig. 7. Relative error on the total energy.

In magnetized plasma, if flow shear exists together with density–temperature (or pressure) gradient, a source of the turbulence, the flow shear may suppress the turbulence driven by pressure gradient relaxation. These shear flows can be self-generated, in which case the Reynolds stress tensor is their main driving term. There is an energy transfer from the turbulent low-frequency electromagnetic (drift waves) fluctuations to these periodic zonal flow fluctuations via either local (inverse energy cascade) or non-local interactions in Fourier space. The back reaction of self-generated shear flow, on

pressure-gradient-driven turbulence, is a key mechanism that governs the turbulent state and the transport, especially it can lead to the formation of transport barriers. In fact many nonlinear simulations show a significant reduction of the transport when zonal flows are present [42,33,29]. In a review of zonal flow phenomena [15], the authors show that poloidal velocity shear plays an important role in regulating (suppressing) turbulent transport. In that case the back reaction of shear flows on turbulence can take the form of random shearing on turbulent eddies, leading to a diffusion of drift waves action in the wave number space k_r. In other words the drift wave spectrum in k_r spreads diffusively. Fig. 8(a) represents the mean poloidal velocity $\langle v_\theta \rangle_{\theta,z} = \partial_r \langle \phi \rangle_{\theta,z}$, the so-called zonal flows, while Fig. 8(b) depicts its corresponding curvature, i.e. its second-order

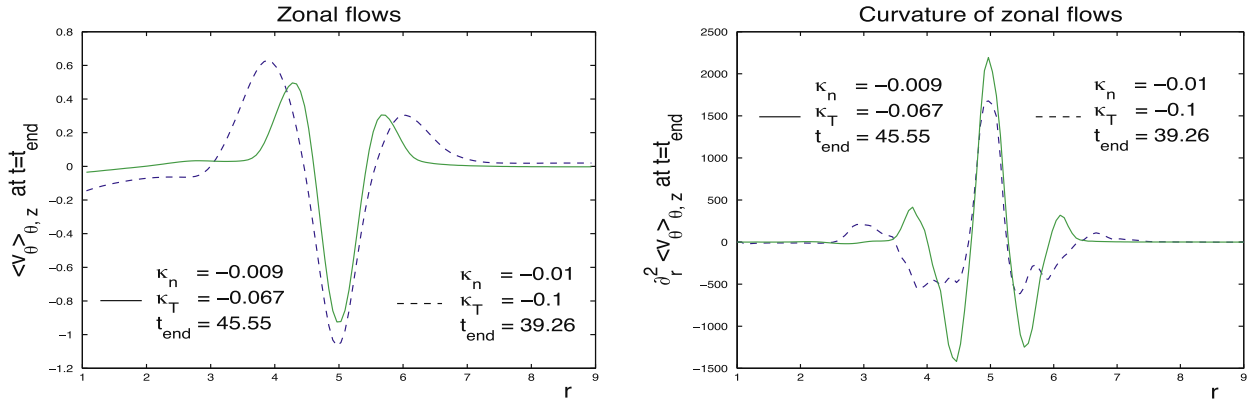

(a) Zonal flows (b) Curvature of zonal flows

Fig. 8. Zonal flows (a), curvature of zonal flows (b), in the nonlinear case.

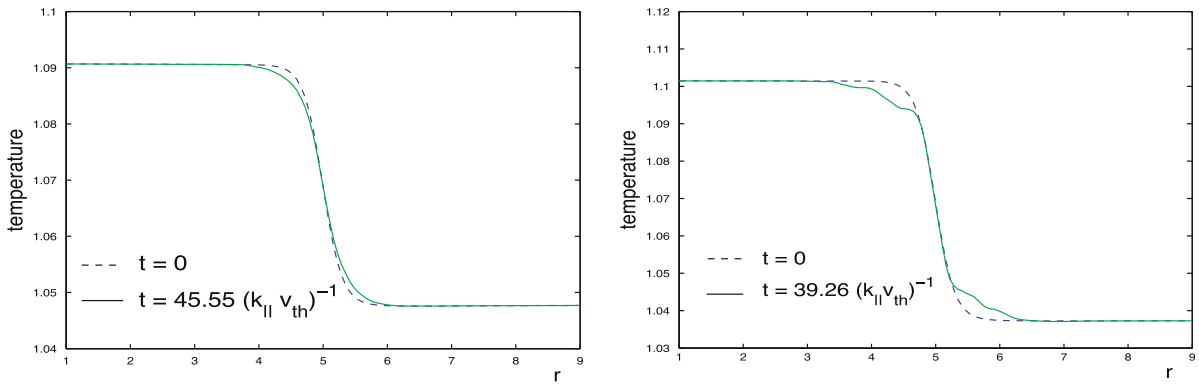

(a) $\kappa_n = -0.009$, $\kappa_T = -0.067$ (b) $\kappa_n = -0.01$, $\kappa_T = -0.1$

Fig. 9. Comparison between the initial and the final radial temperature profile in the nonlinear case.

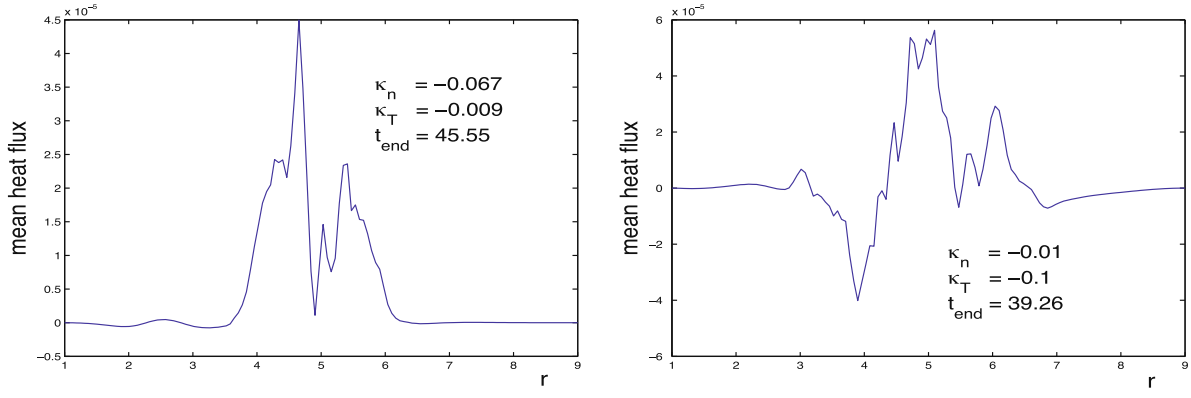

(a) $\kappa_n = -0.009$, $\kappa_T = -0.067$ (b) $\kappa_n = -0.01$, $\kappa_T = -0.1$

Fig. 10. Mean heat flux profile in the nonlinear case.

radial derivative. Fig. 8 indicates the presence of a poloidal velocity shear layer centered at $r = r_0 = 5$. From Figs. 9 and 8 we observe that the maximum of the temperature gradient, the mean sheared flow, and the curvature of zonal flows are at the same location $r = r_0$. These results are in agreement with those obtained with the full-f gyrokinetic Vlasov code GYSELA [25,41]. Moreover in Fig. 10 we see a sensible reduction of the turbulent heat flux at the location $r = r_0$. In agreements with linear perturbative theory and other numerical simulations [41], this suggests that any strong temperature gradient

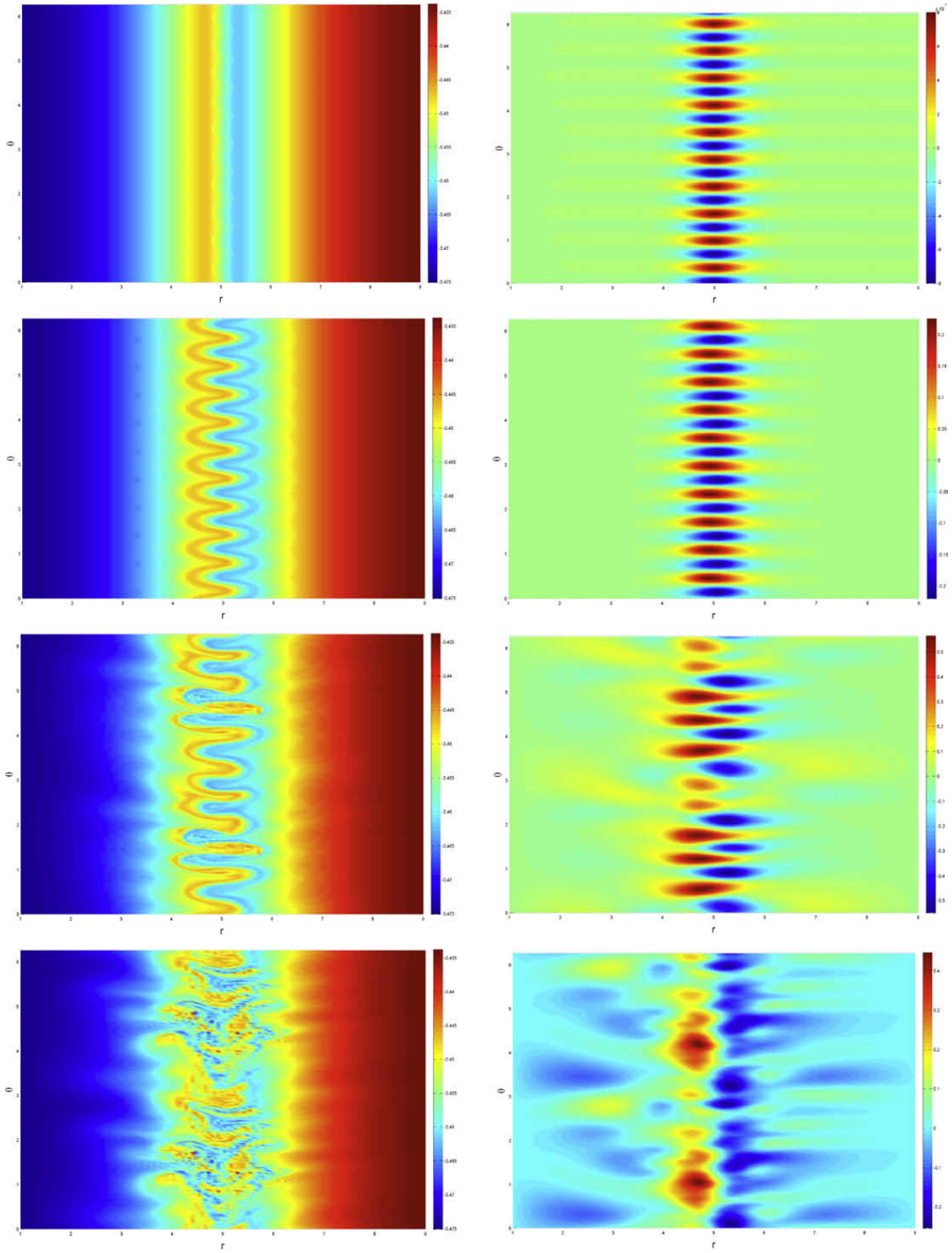

(a) (r,θ)-slice of the contour v_1^- (b) (r,θ)-slice of the electrical potential ϕ

Fig. 11. (a) (r,θ)-slice at a given azimuthal position z_0 of the contour v_1^-, remembering that the contour $v_1^-(t,r,\theta,z)$ belongs to a three-dimensional space; (b) the electrical potential ϕ at times $t = 9.42, t = 18.84, t = 37.70$ and $t = 45.55$ for $\kappa_n = -0.009$ and $\kappa_T = -0.067$.

associated with a maximum of zonal flow curvature can survive, possibly leading to a transport barrier. The existence of a thin poloidal velocity shear layer can also be observed on the (r,θ)-slice of the electrical potential at a given azimuthal position $z = z_0$ in Fig. 11(b) at time $t = 45.55$ and in Fig. 12(b) at times $t = 26.70$ and $t = 39.26$.

In Figs. 11 and 12 we see an example of what a half bag, for instance the v_1^- contour, and the electric potential look like. The linear phase is obviously observed at time $t = 9.42$ in Fig. 11, and time $t = 4.71$ in Fig. 12. We next notice the beginning of the nonlinear phase at time $t = 18.84$ in Fig. 11, and time $t = 9.42$ in Fig. 12. Thence we are in the nonlinear regime, where we observe zonal flows presence from the electrical potential and the development of the filamentation phenomenon from

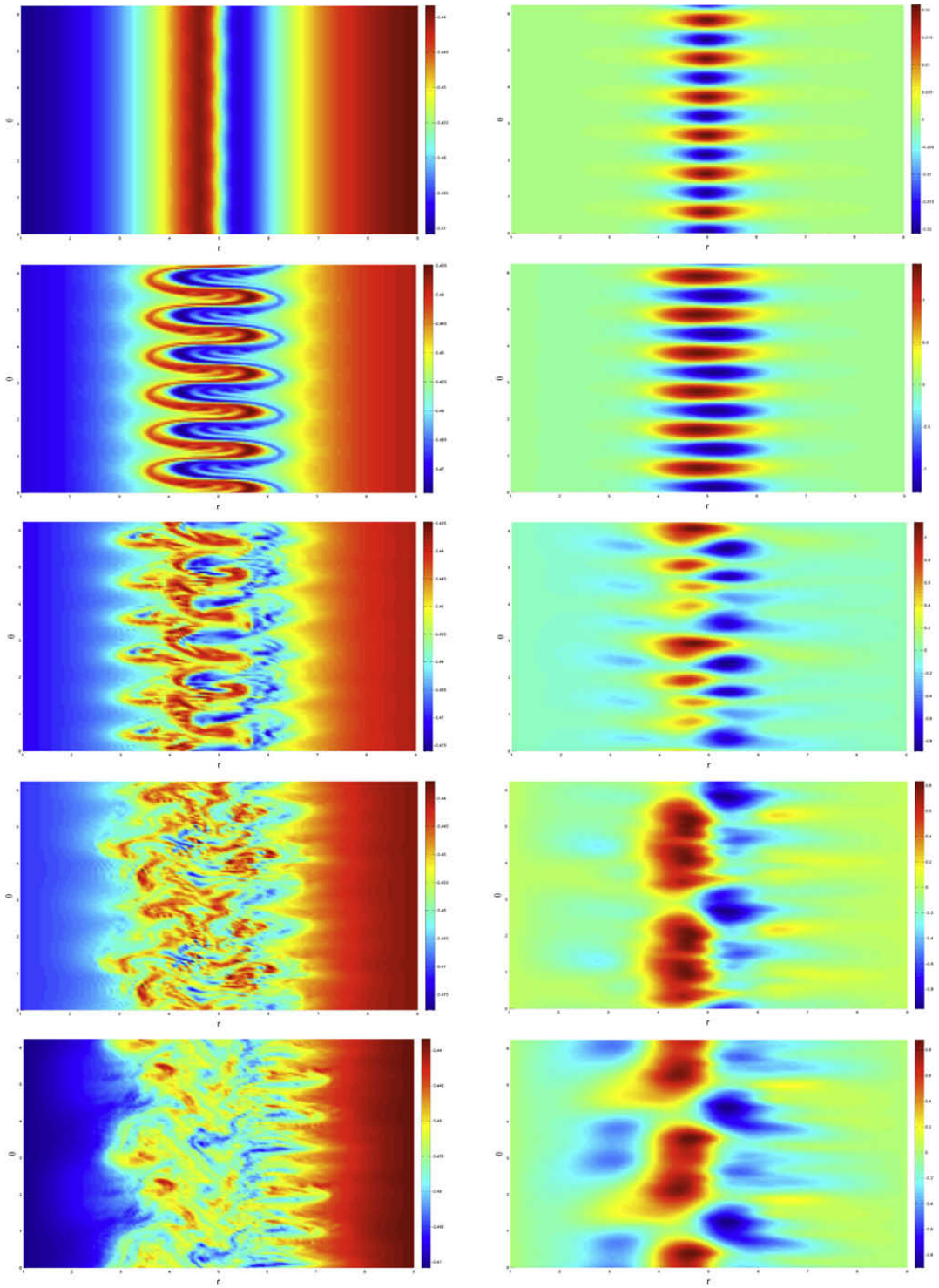

(a) (r,θ)-slice of the contour v_1^- (b) (r,θ)-slice of the electrical potential ϕ

Fig. 12. (a) (r,θ)-slice at a given azimuthal position z_0 of the contour v_1^-, remembering that the contour $v_1^-(t,r,\theta,z)$ belongs to a three-dimensional space; (b) the electrical potential ϕ at times $t = 4.71, t = 9.42, t = 17.27, t = 26.70$ and $t = 39.26$ for $\kappa_n = -0.01$ and $\kappa_T = -0.1$.

the (r,θ)-slice of the contour v_1^{-1} at a given azimuthal position z_0. The incompressible nature of the flow in the transverse direction leads to this filamentation phenomenon, also observed in phase-space for Vlasov-type equation. It could lead to numerical problems in long time simulations, because this phenomenon produces a growing of small scale poloidal structures. When these small scales become smaller than the space grid size, informations are lost and unknowns are smoothed which corresponds to an addition of non physical and nonlinear diffusion operator like effects. Even if a refinement of the mesh in the poloidal direction will improve the treatment of small scales, it will always be not sufficient as the filamentation mechanism generates smaller and smaller scale structures as time goes on. Nevertheless, if we take into account finite Larmor radius effects, it introduces a natural and physical filter or regularization mechanism which consists in an averaging procedure in the transverse direction. Therefore the addition of gyroaverage operator (4) tends to limit the development of small scales structures. As an example, Figs. 13–15 give an illustration of the effects of the gyroaverage operator. In Fig. 13(a) we observe that the growth rate is a little bit smaller than one obtained without gyroaveraging, as it is well known while in Fig. 13(b) the level of the turbulent heat flux and electrical potential energy keeps the same level. In Figs. 14 and 15 we notice that the transversal structures are a little bit more regularized, but actually it is not significant as the simulation need to run enough far in time to observe the gyroaveraging effect and because we only take one adiabatic invariant $\mu = \mu_0$.

6. Perspectives

In this paper we have considered the water-bag weak solution of the Vlasov gyrokinetic equation, resulting in the birth of the gyro-water-bag model. We have also derived a self-consistent quasilinear model from the nonlinear gyro-water-bag model, to cross-check the linear regime of the ITG instability. Each model has been solved with a different numerical method to state the reliability of the models and the associated numerical schemes. Not only the quasilinear model is in agreement

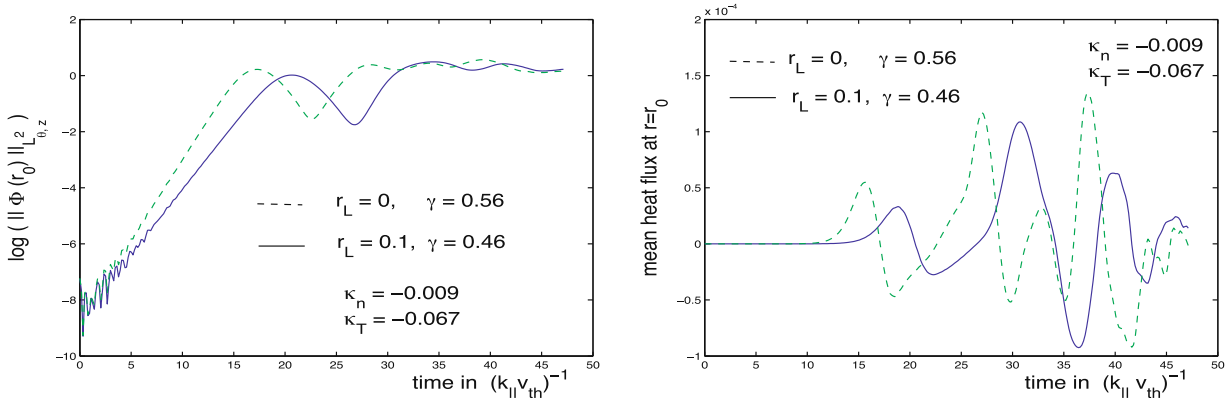

(a) L^2-norm of ϕ at $r = r_0$ (b) Mean heat flux at $r = r_0$

Fig. 13. Comparison of the L^2-norm of the electrical potential (a) and the mean heat flux (b) at $r = r_0$ for $\kappa_n = -0.009$, $\kappa_T = -0.067$ when the gyroaverage operator is considered ($r_L = 0.1$) or not ($r_L = 0$).

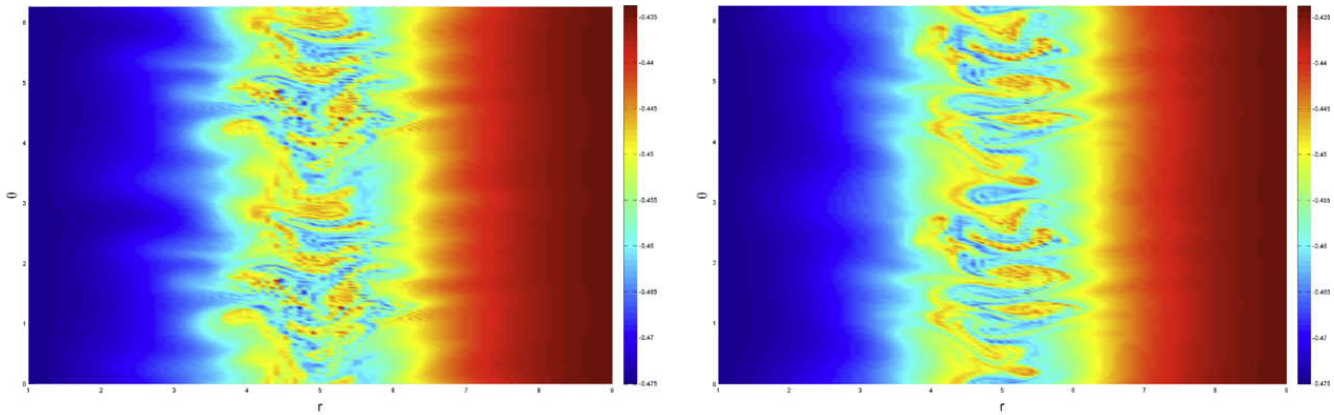

(a) (r,θ)-slice of the contour v_1^- with $r_L = 0$ (b) (r,θ)-slice of the contour v_1^- with $r_L = 0.1$

Fig. 14. Comparison of the (r,θ)-slice at a given azimuthal position z_0 of the contour v_1^- when the gyroaverage operator is not considered (a) and when it is (b) for $\kappa_n = -0.009$, $\kappa_T = -0.067$ at time $t = 45.55$.

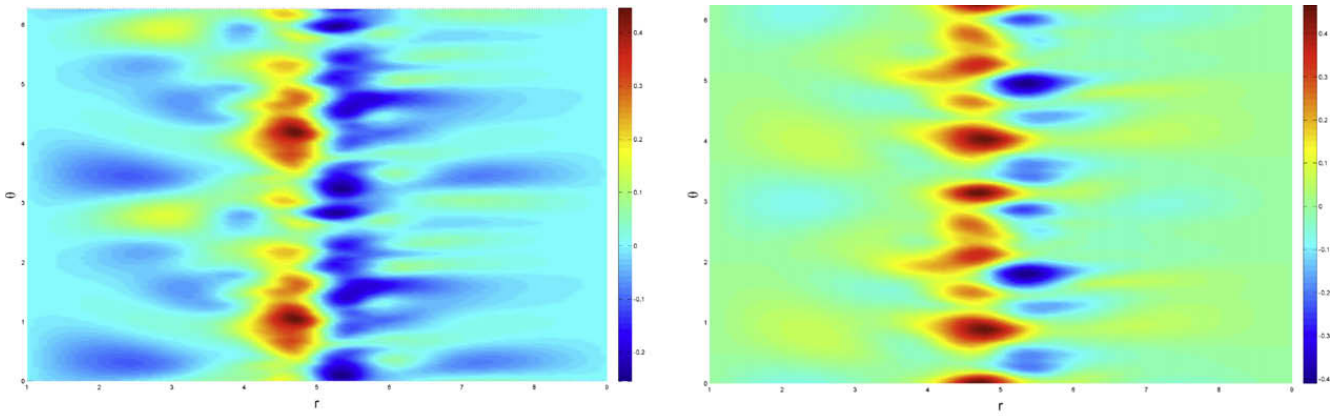

(a) (r,θ)-slice of the potential ϕ with $r_L = 0$ (b) (r,θ)-slice of the potential ϕ with $r_L = 0.1$

Fig. 15. Comparison of the (r,θ)-slice at a given azimuthal position z_0 of the electrical potential ϕ when the gyroaverage operator is not considered (a) and when it is (b) for $\kappa_n = -0.009$, $\kappa_T = -0.067$ at time $t = 45.55$.

with the nonlinear model in the linear stage, but also it proves to be a good approximation of the full nonlinear model since the quasilinear estimate of the turbulent transport is of the same order as the nonlinear one. Moreover the results obtained with the full nonlinear gyro-water-bag model, such as the existence of both the radial turbulence regime and transport barriers for instance poloidal zonal flows, are qualitatively in agreement with the results observed with the full-*f* gyrokinetic Vlasov code GYSELA [41]. Quantitative comparisons with a gyrokinetic Vlasov code, like GYSELA for example, are still beyond the scope of the present paper, but will be the starting point of further studies.

References

[1] H.L. Berk, K.V. Roberts, The water bag model, Methods in Computational Physics, vol. 9, Academic Press, 1970.
[2] P. Bertrand, M.R. Feix, Non linear electron plasma oscillation: the "water bag model", Phys. Lett. 28A (1968) 68–69.
[3] P. Bertrand, M.R. Feix, Frequency shift of non linear electron plasma oscillation, Phys. Lett. 29A (1969) 489–490.
[4] P. Bertrand, Contribution à l'étude de modèles mathématiques de plasmas non collisionels, Ph.D. Thesis, Universitde Nancy, France, 1972.
[5] P. Bertrand, J.P. Doremus, G. Baumann, M.R. Feix, Stability of inhomogeneous two-stream plasma with a water-bag model, Phys. Fluids 15 (1972) 1275–1281.
[6] P. Bertrand, M. Gros, G. Baumann, Nonlinear plasma oscillations in terms of multiple-water-bag eigenmodes, Phys. Fluids 19 (1976) 1183–1188.
[7] N. Besse, N.J. Mauser, E. Sonnendrücker, Numerical approximation of self-consistent Vlasov models for low-frequency electromagnetic phenomena, Int. J. Appl. Math. Comput. Sci. 17 (2007) 101–114.
[8] N. Besse, P. Bertrand, Quasilinear analysis of the gyro-water-bag model, Europhys. Lett. 83 (2008) 25003.
[9] A.J. Brizard, T.S. Hahm, Foundations of nonlinear gyrokinetic theory, Rev. Mod. Phys. 79 (2007) 421–468.
[10] A.J. Brizard, New variational principle for the Vlasov–Maxwell equations, Phys. Rev. Lett. 84 (2000) 5768–5771.
[11] J. Candy, R.E. Waltz, An Eulerian gyrokinetic-Maxwell solver, J. Comput. Phys. 186 (2003) 545–581.
[12] B. Cockburn, C.-W. Shu, Runge–Kutta discontinuous Galerkin methods for convection-dominated problems, J. Sci. Comput. 16 (2001) 173–261.
[13] D.C. DePackh, The water-bag model of a sheet electron beamy, J. Electron. Control 13 (1962) 417–424.
[14] G. Depret, X. Garbet, P. Bertrand, A. Ghizzo, Trapped-ion driven turbulence in tokamak plasmas, Plasma Phys. Controlled Fus. 42 (2000) 949–971.
[15] P.H. Diamond, S.-I. Itoh, K. Itoh, T.S. Hahm, Zonal flows in plasma – a review, Plasma Phys. Controlled Fus. 47 (2005) R35–R161.
[16] W. Dorland, F. Jenko, M. Kotschenreuther, B.N. Rogers, Electron temperature gradient turbulence, Phys. Rev. Lett. 85 (2000) 5579–5582.
[17] W. Dorland, G.W. Hammett, Gyrofluid turbulence models with kinetic effects, Phys. Fluids B 5 (1993) 812–835.
[18] A.M. Dimits et al, Comparisons and physics basis of tokamak transport models and turbulence simulations, Phys. Plasmas 7 (2003) 969–983.
[19] D.H.E. Dubin, J.A. Krommes, C. Oberman, W.W. Lee, Nonlinear gyrokinetic equations, Phys. Fluids 26 (1983) 3524–3535.
[20] M.R. Feix, F. Hohl, L.D. Staton, in: Kalmann, Feix (Eds.), Nonlinear Effects in Plasmas, Gordon and Breach, 1969, pp. 3–21.
[21] U. Finzi, Accessibility of exact nonlinear states in water-bag model computer experiments, Plasma Phys. 14 (1972) 327–338.
[22] E.A. Frieman, L. Chen, Nonlinear gyrokinetic equations for low-frequency electromagnetic waves in general plasma equilibria, Phys. Fluids 25 (1982) 502–508.
[23] X. Garbet, R.E. Waltz, Action at distance an Bohm scaling of turbulence in tokamaks, Phys. Plasmas 3 (1996) 1898–1907.
[24] S. Gottlieb, C.-W. Shu, E. Tadmor, Strong stability-preserving high-order time discretization methods, SIAM Rev. 43 (2001) 89–112.
[25] V. Grandgirard, M. Brunetti, P. Bertrand, N. Besse, X. Garbet, et al, A drift-kinetic semi-Lagrangian 4D code for ion turbulence simulation, J. Comput. Phys. 217 (2006) 395–423.
[26] T.S. Hahm, Nonlinear gyrokinetic equations for tokamak microturbulence, Phys. Fluids 31 (1988) 2670–2673.
[27] F.R. Hansen, G. Knorr, J.P. Lynov, H.L. Pécseli, J.J. Rasmussen, A numerical plasma simulation including finite Larmor radius effects to arbitrary order, Plasma Phys. Controlled Fus. 31 (1989) 173–183.
[28] Y. Idomura, S. Tokuda, Y. Kishimoto, Global gyrokinetic simulation of ion temperature gradient driven turbulence in plasmas using a canonical Maxwellian distribution, Nucl. Fus. 43 (2003) 234–243.
[29] Y. Idomura, M. Wakatani, S. Tokuda, Stability of $E \times B$ zonal flow in electron temperature gradient driven turbulence, Phys. Plasmas 7 (2000) 3551–3556.
[30] G.E. Karniadakis, S.J. Sherwin, Spectral/hp Element Methods in CFD, Oxford University Press, 1999.
[31] G. Knorr, H.L. Pécseli, Asymptotic state of the finite-Larmor-radius guiding-center plasma, J. Plasma Phys. 41 (1989) 157–170.
[32] W.W. Lee, Gyrokinetic approach in particle simulation, Phys. Fluids 26 (1983) 556–562.
[33] Z. Lin, T.S. Hahm, W.W. Lee, W.M. Tang, R.B. White, Gyrokinetic simulations in general geometry and applications to collisional damping of zonal flows, Phys. Plasmas 7 (2000) 1857–1862.

[34] G. Manfredi, M. Ottaviani, Gyro–Bohm scaling of ion thermal transport from global numerical simulations of ion-temperature-gradient-driven turbulence, Phys. Rev. Lett. 79 (1997) 4190–4193.
[35] P. Morel, E. Gravier, N. Besse, R. Klein, A. Ghizzo, P. Bertrand, et al, Gyro kinetic modeling: a multi-water-bag approach, Phys. Plasmas 14 (2007) 112109.
[36] P. Morel, E. Gravier, N. Besse, P. Bertrand, The water bag model and gyrokinetic applications, Commun. Nonlinear Sci. Numer. Simul. 13 (2008) 11–17.
[37] M. Navet, P. Bertrand, Multiple "water-bag" model and Landau damping, Phys. Lett. 34A (1971) 117–118.
[38] H. Nordman, J. Weiland, A. Jarmén, Simulation of toroidal drift mode turbulence driven by temperature gradients and electron trapping, Nucl. Fus. 30 (1990) 983–996.
[39] S.E. Parker, W.W. Lee, R.A. Santoro, Gyrokinetic simulation of ion temperature gradient driven turbulence in 3D toroidal geometry, Phys. Rev. Lett. 71 (1993) 2042–2045.
[40] Y. Sarazin, V. Grandgirard, E. Fleurence, X. Garbet, Ph. Ghendrih, P. Bertrand, G. Depret, Kinetic features of interchange turbulence, Plasma Phys. Controlled Fus. 47 (2005) 1817–1839.
[41] Y. Sarazin, V. Grandgirard, G. Dif-Pradalier, X. Garbet, Ph. Ghendrih, Interplay between transport barriers and density gradient, Phys. Plasmas 13 (2006) 092307.
[42] R.D. Sydora, V.K. Decyk, J.M. Dawson, Fluctuation-induced heat transport results from a large global 3D toroidal particle simulation model, Plasma Phys. Controlled Fus. 38 (1996) A281–A294.
[43] R.E. Waltz, Three-dimensional global numerical simulation of ion temperature gradient mode turbulence, Phys. Fluids 31 (1988) 1962–1967.